

1 Highlights

2 **Improved consistency between the modelling of ocean optics, bio-**  
3 **geochemistry and physics, and its impact on the North-West Eu-**  
4 **ropean Shelf seas**

5 Jozef Skákala, Jorn Bruggeman, David Ford, Sarah Wakelin, Anil Akpınar,  
6 Tom Hull, Jan Kaiser, Benjamin R. Loveday, Charlotte A.J. Williams, Ste-  
7 fano Ciavatta

- 8 • We established two-way coupling between biogeochemistry and physics.
- 9 • We assessed the impact of the coupling in free and assimilative exper-  
10 iments.
- 11 • The two-way coupling improves the simulated biogeochemistry on the  
12 NWE Shelf.
- 13 • We recommend to implement this development into the operational  
14 system.

15 Improved consistency between the modelling of ocean  
16 optics, biogeochemistry and physics, and its impact on  
17 the North-West European Shelf seas

18 Jozef Skákala<sup>a,b</sup>, Jorn Bruggeman<sup>a</sup>, David Ford<sup>c</sup>, Sarah Wakelin<sup>d</sup>, Anil  
19 Akpınar<sup>d</sup>, Tom Hull<sup>e,f</sup>, Jan Kaiser<sup>f</sup>, Benjamin R. Loveday<sup>g</sup>, Charlotte A.J.  
20 Williams<sup>d</sup>, Stefano Ciavatta<sup>a,b</sup>

<sup>a</sup>*Plymouth Marine Laboratory, Prospect Place, The Hoe, Plymouth, PL1 3DH, United Kingdom*

<sup>b</sup>*National Centre for Earth Observation, Prospect Place, The Hoe, Plymouth, PL1 3DH, United Kingdom*

<sup>c</sup>*Met Office, FitzRoy Road, Exeter, EX1 3PB, United Kingdom*

<sup>d</sup>*National Oceanography Centre, Joseph Proudman Building, 6 Brownlow Street, Liverpool, L3 5DA, United Kingdom*

<sup>e</sup>*Centre for Environment, Fisheries and Aquaculture Science, Lowesoft, NR33 0HT, United Kingdom*

<sup>f</sup>*Centre for Ocean and Atmospheric Science, University of East Anglia, Norwich, NR4 7TJ, United Kingdom*

<sup>g</sup>*Innoflair UG, Richard-Wagner-Weg 35, Darmstadt, 64287, Germany*

---

21 **Abstract**

We use a recently developed spectrally resolved bio-optical module to better represent the interaction between the incoming irradiance and the heat fluxes in the upper ocean within the (pre-)operational physical-biogeochemical model on the North-West European (NWE) Shelf. The module attenuates light based on the simulated biogeochemical tracer concentrations, and thus introduces a two-way coupling between the biogeochemistry and physics. We demonstrate that in the late spring-summer the two-way coupled model heats up the upper oceanic layer, shallows the mixed layer depth and influences the mixing in the upper ocean. The increased heating in the upper oceanic layer reduces the convective mixing and improves by  $\sim 5$  days the timing of the late phytoplankton bloom of the ecosystem model. This improvement is relatively small compared with the existing model bias in bloom timing, but sufficient to have a visible impact on model skill. We show that the changes to the model temperature and salinity introduced by the module have mixed

impact on the physical model skill, but the skill can be improved by assimilating the observations of temperature, salinity and chlorophyll concentrations into the model. However, in the situations where we improved the simulation of temperature, either via the bio-optical module, or via assimilation of temperature and salinity, we have shown that we also improved the simulated oxygen concentration as a result of the changes in the simulated air-sea gas flux. Overall, comparing different 1-year experiments showed that the best model skill is achieved with joint physical-biogeochemical assimilation into the two-way coupled model.

22 *Keywords:* two-way coupled physical-biogeochemical model, ocean  
23 chlorophyll concentration, sea surface temperature, phytoplankton spring  
24 bloom, North-West European Shelf (10E-10W, 40N-68N), data assimilation

---

## 25 **1. Introduction**

26 Physical-biogeochemical ocean models are an essential element in mon-  
27 itoring and forecasting of global and shelf-sea ecosystem indicators ([1, 2]).  
28 However, coupled physical-biogeochemical marine modelling is a complex un-  
29 dertaking and a common way to simplify coupled models is to neglect the  
30 impact of the biogeochemical model state on physics ([3, 2]). Although ma-  
31 rine ecosystem models often neglect the coupling from the biogeochemical  
32 model state to physics, there are number of established mechanisms through  
33 which biogeochemistry influences physics and climate ([4, 1, 2]): (i) marine  
34 ecosystems play an essential part in the carbon cycle through biological and  
35 microbial carbon pump, influencing atmospheric carbon concentrations and  
36 the Earth surface temperature, (ii) phytoplankton influences oceanic albedo  
37 (e.g. [5]) having an overall impact on the radiative terms and Earth energy  
38 budget, (iii) some biogeochemical tracers influence light attenuation, mod-  
39 ifying the short-wave heat fluxes in the water column and therefore ocean  
40 stratification ([6, 7, 8, 9, 10, 11, 12, 13, 14]), and (iv) marine ecosystems have  
41 an impact on cloud condensation nuclei through the production of dimethyl  
42 sulfide (DMS, [15, 16, 17, 18]), or more directly via bubble formation ([19]).  
43 The size of life’s impact on Earth’s physics has been subject to much de-  
44 bate ([2]), often in connection with “the Gaia hypothesis” ([20, 21]), which  
45 proposes that life plays a central role in regulating climate.

46 For coupled physical-biogeochemical marine models the main source of  
47 impact of ecosystems on physics is through the absorption and backscatter-

48 ing of short-wave radiation by some biogeochemical substances in the sea  
49 water (e.g. [10]). The presence of optically active tracers, such as chloro-  
50 phyll, suspended particulate matter (SPM), or colored dissolved organic mat-  
51 ter (CDOM), in the oceanic upper layer increases light attenuation near the  
52 oceanic surface, warms the sea temperature in the upper ocean, which typi-  
53 cally influences the mixing in the upper oceanic layer (e.g. [6]), e.g. shallow-  
54 ing the thermocline and the mixed layer depth (MLD). The changes to the  
55 vertical mixing can in turn impact the biogeochemical model, by influencing  
56 the nutrient concentrations and growth conditions in the upper ocean.

57 In this work we focus on the Copernicus Marine Environmental Moni-  
58 toring Service (CMEMS) operational system for the North-West European  
59 (NWE) Shelf biogeochemistry, which is of a substantial societal benefit, as the  
60 NWE Shelf is a key region for fisheries, and an important contributor to the  
61 global carbon cycle ([22, 23, 24]). The presently used physical-biogeochemical  
62 operational model for the NWE Shelf is the marine physical model Nucleus  
63 for European Modelling of the Ocean (NEMO, [25]) coupled through the  
64 Framework for Aquatic Biogeochemical Models (FABM, [26, 27]) to the Euro-  
65 pean Regional Seas Ecosystem Model (ERSEM, [28, 29, 30]). NEMO-FABM-  
66 ERSEM drives its physics and biogeochemistry by two separate irradiance  
67 modules: (i) the physical model calculates heat fluxes from the incoming  
68 net short-wave radiation (SWR) split into two wavebands, the 400-700nm  
69 visible band reduced through attenuation obtained from a monthly climatol-  
70 ogy of a satellite surface  $K_d$  product at 490nm wavelength (European Space  
71 Agency product version 2.0, <https://www.esa-oceancolour-cci.org/>), and the  
72 UV/infrared band reduced with a preset attenuation with an e-folding scale  
73 of 0.35m, (ii) the biogeochemical model reduces incoming photosynthetic ac-  
74 tive radiation (PAR) by taking into account both absorption and backscat-  
75 tering by the sea water and the simulated Phytoplankton Functional Types  
76 (PFTs), and also by including absorption by Particulate Organic Matter  
77 (POM), CDOM and sediment represented by an external satellite product  
78 (for details see [29, 31]). The presently used scheme means that, although  
79 some impact of biogeochemical tracers on the physical model is implicitly  
80 included in the 490nm  $K_d$  satellite climatology, there is no feedback from the  
81 biogeochemical model state to the simulated physics.

82 In [31] we implemented into ERSEM a stand-alone bio-optical module  
83 (based on OASIM, [32, 33, 34]), that resolves irradiance spectrally and splits  
84 the irradiance into diffuse and direct streams ([35]). The module then propa-  
85 gates irradiance through the water column, based on attenuation by sea water

86 and the biogeochemical substances in the water. The new module drove only  
87 the biogeochemical part of the coupled NEMO-FABM-ERSEM model, sub-  
88 stantially improving the underwater irradiance, but without a major impact  
89 on the ERSEM model skill on the NWE Shelf ([31]). This version of NEMO-  
90 FABM-ERSEM model will be used in the present study as a reference run  
91 and will be called a “one-way coupled model”. In this work we expand the  
92 development implemented in [31] by using the bio-optical module to drive  
93 both the biogeochemistry and the physics (i.e. heating by light absorption).  
94 Since the physical heat fluxes will be driven by the underwater irradiance  
95 that is attenuated by biogeochemical substances, the module establishes an  
96 important feedback from the biogeochemical model to physics. We will fur-  
97 ther call this new implementation a “two-way coupled model”, to distinguish  
98 it from the “one-way coupled” reference run.

99 This work aims at answering two main questions: (i) What is the size  
100 of the biogeochemical impact on the marine physics within the NWE Shelf?  
101 (ii) Does the impact of the spectrally resolved bio-optical module on physics  
102 lead to more internally consistent ecosystem dynamics on the NWE Shelf,  
103 and hence, an improvement in the operational biogeochemical model skill?  
104 Those two questions are answered both in the context of free simulations  
105 and also in the context of (physical, biogeochemical, coupled) assimilative  
106 runs. The second question is particularly relevant: It has been established  
107 that NEMO-FABM-ERSEM displays on the NWE Shelf late and intense  
108 spring blooms ([31, 36]). Since a spring bloom is a major ecosystem driver  
109 ([37, 38]), the simulated late blooms severely limit the ecosystem model skill  
110 ([31, 36]). Although many factors can influence the bloom timing (including  
111 biological drivers, such as zooplankton grazing, e.g. [39]), one of the leading  
112 hypotheses for how phytoplankton blooms are triggered in the North Atlantic  
113 is based on the interplay between PAR and an effective mixing depth (the  
114 critical turbulence hypothesis, [40, 41]), i.e. the bloom sets in when the  
115 effective mixing depth becomes fully contained within the euphotic layer  
116 ([42]). Within the scope of the critical turbulence hypothesis, the delay in  
117 bloom timing could then be explained by multiple components within the  
118 physical-biogeochemical coupled model: (a) atmospheric wind stress forcing,  
119 (b) model upper-ocean mixing scheme, (c) vertical stratification (thermocline  
120 and pycnocline), (d) incoming surface PAR, (e) underwater light attenuation,  
121 (f) the phytoplankton growth response to light (e.g. model parameters, such  
122 as P-I curves, maximum PFT chlorophyll-to-carbon ratios). In [31] we have  
123 addressed to a varying degree the points (d) and (e) without a significant

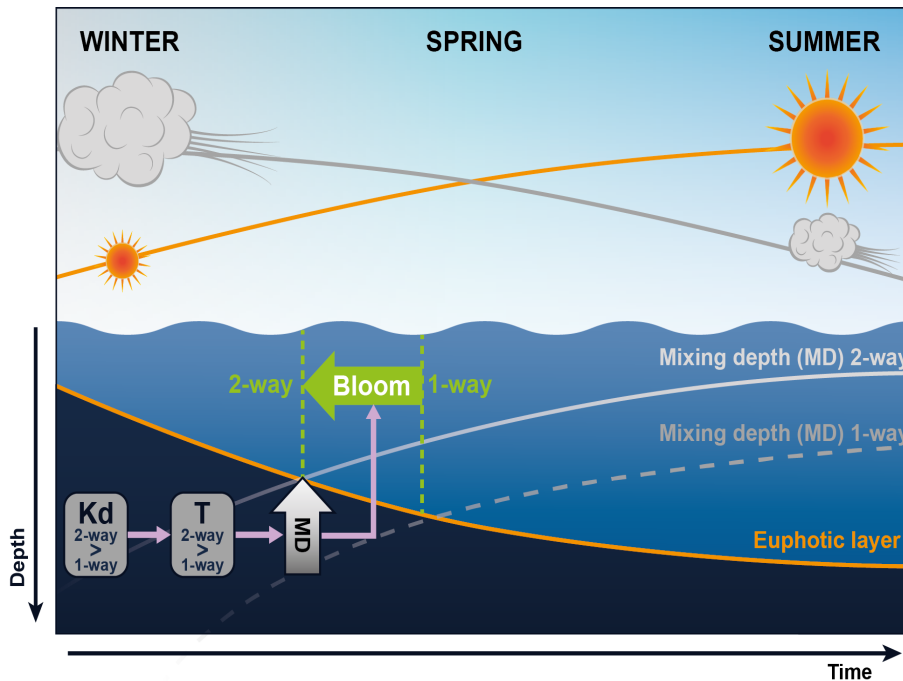


Figure 1: A schematic representation of the hypothesis about the impact of the two-way coupled model on the timing of the simulated bloom.

124 impact on the bloom timing. However, [31] observed that attenuation of  
 125 light based on the satellite  $K_d$  product for the 490 nm wavelength is most  
 126 likely an underestimate of the total PAR absorbed in the upper oceanic layer.  
 127 Calculating heat fluxes using the bio-optical module is therefore expected to  
 128 produce extra heat in the upper oceanic layer (Fig.5 of [31]), which is thought  
 129 to shallow the MLD, but it can also reduce turbulent convective mixing near  
 130 the oceanic surface ([43, 44]). The hypothesis tested in this work (see Fig.1) is  
 131 that the reduced convective mixing can lead to a shallower turbulent mixing  
 132 depth and help trigger an earlier phytoplankton bloom, as suggested by the  
 133 critical turbulence hypothesis ([40, 44]). The biogeochemical feedback to the  
 134 simulated physics could therefore improve the ERSEM skill on the NWE  
 135 Shelf.

## 136 2. Methods

### 137 2.1. The physical model: NEMO

138 The NEMO ocean physics component (OPA) is a finite difference, hydro-  
139 static, primitive equation ocean general circulation model ([25]). The NEMO  
140 configuration used in this study is similar to the one used by [45, 46, 31], and  
141 identical to the configuration used in [36]: we use the CO6 NEMO version,  
142 based on NEMOv3.6, a development of the CO5 configuration explained in  
143 detail by [47]. The model has 7 km spatial resolution on the Atlantic Margin  
144 Model (AMM7) domain using a terrain-following  $z^* - \sigma$  coordinate system  
145 with 51 vertical levels ([48]). The lateral boundary conditions for physical  
146 variables at the Atlantic boundary were taken from the outputs of the Met  
147 Office operational 1/12° North Atlantic model (NATL12, [49]); the Baltic  
148 boundary values were derived from a reanalysis produced by the Danish Me-  
149 teorological Institute for CMEMS. We use annually varying river discharge  
150 based on data from [50].

151 The model was forced at the surface by atmospheric fluxes provided by  
152 an hourly and 31km resolution realisation (HRES) of the ERA5 data-set  
153 (<https://www.ecmwf.int/>). In case of the one-way coupled model the ERA5  
154 fluxes provide also the total incoming net shortwave radiation whose visible  
155 fraction is attenuated inside the water column based on the  $K_d$  for 490nm  
156 wavelength supplied by a monthly climatology from an Ocean Color - Climate  
157 Change Initiative (OC-CCI) product of European Space Agency (ESA), ver-  
158 sion 4.1 (<https://www.esa-oceancolour-cci.org/>). For the two-way coupled  
159 model the incoming net short-wave radiation is decomposed into direct and  
160 diffuse streams and spectrally resolved, and is provided by the bio-optical  
161 module ([31]) that will be described later in the ecosystem model section.  
162 The direct and diffuse streams are attenuated throughout the water column  
163 by the bio-optical module, and subsequently integrated by NEMO to calcu-  
164 late the heating within each vertical layer.

### 165 2.2. The ecosystem model: ERSEM

166 ERSEM ([28, 29]) is a lower trophic level ecosystem model for marine bio-  
167 geochemistry, pelagic plankton, and benthic fauna ([51]). The model splits  
168 phytoplankton into four functional types largely based on their size ([28]): pi-  
169 cophytoplankton, nanophytoplankton, diatoms and dinoflagellates. ERSEM  
170 uses variable stoichiometry for the simulated plankton groups ([52, 53]) and  
171 each Phytoplankton Functional Type (PFT) biomass is represented in terms

172 of chlorophyll, carbon, nitrogen and phosphorus, with diatoms also repre-  
173 sented by silicon. ERSEM predators are composed of three zooplankton  
174 types (mesozooplankton, microzooplankton and heterotrophic nanoflagel-  
175 lates), with organic material being decomposed by one functional type of  
176 heterotrophic bacteria ([29]). The ERSEM inorganic component consists of  
177 nutrients (nitrate, phosphate, silicate, ammonium and carbon) and dissolved  
178 oxygen. The carbonate system is also included in the model ([54]).

179 We applied in this study the ERSEM configuration from [36], based on a  
180 new ERSEM version 20.10, which has an updated benthic component with  
181 respect to [29]. The ERSEM parametrization is identical to the one described  
182 in [29]. The Atlantic boundary values for nitrate, phosphate, silicate and  
183 oxygen were taken from World Ocean Atlas ([55]) and dissolved inorganic  
184 carbon from the GLODAP gridded dataset ([56, 57]), while plankton and  
185 detritus variables were set to have zero fluxes at the Atlantic boundary.

186 The irradiance at the ocean surface was calculated using the bio-optical  
187 module implemented into the NEMO-FABM-ERSEM AMM7 configuration  
188 by [31]. The bio-optical module resolves irradiance spectrally and distin-  
189 guishes between downwelling direct and diffuse streams. The module is  
190 forced by the ERA5 atmospheric inputs (<https://www.ecmwf.int/>) for to-  
191 tal vertically integrated ozone, water vapour, cloud cover, cloud liquid water  
192 and sea-level air pressure, as well as by a satellite product for aerosol op-  
193 tical thickness (MODerate resolution Imaging Spectroradiometer, MODIS,  
194 <https://modis.gsfc.nasa.gov/data/dataproduct>), and also by data for surface  
195 wind speed, air humidity, and air temperature, all provided by the NEMO at-  
196 mospheric (ERA5) forcing. The attenuation of the irradiance was described  
197 in detail by [31], here it is briefly summarized: The module distinguishes  
198 between the absorption and backscattering by the sea water and the 4 PFTs  
199 based on the model of [58]. The scheme for the underwater irradiance was  
200 based on [33], i.e. the irradiance was resolved at 33 wavelengths in the  
201 250 - 3700nm range, and so were the wavelength-dependent absorption and  
202 backscattering coefficients for clear water and PFTs. Although we included  
203 the impact of backscattering on the light attenuation, similarly to [31], we  
204 did not explicitly track the upwelling stream. Besides the clear sea water  
205 and PFTs, we included into the light attenuation also the absorption by  
206 POM, CDOM and sediment, which was (the same as in [31]) forced by an  
207 external product extrapolated from the 443nm data of [59]. The bio-optical  
208 module was extensively validated in [31], and was shown to be skilled in its  
209 representation of SWR, PAR and the underwater irradiances.

210 *2.3. Observations: assimilated and validation data*

211 *2.3.1. Assimilated data*

212 In the physical data assimilation component we have included: a) sea  
213 surface temperature data from the GCOM-W1/AMSR-2, NOAA/AVHRR,  
214 MetOp/AVHRR, MSG/SEVIRI, Sentinel-3/SLSTR, Suomi-NPP/VIIRS satel-  
215 lite products and in situ SST observations from ships, surface drifters and  
216 moorings, distributed over the Global Telecommunication System (GTS) in  
217 near-real time, b) temperature and salinity from the EN4 dataset ([60]),  
218 which includes in situ profiles from Argo floats, fixed moored arrays, XBTs,  
219 CTDs, gliders, marine mammals, and c) temperature and salinity data from  
220 a specific Slocum glider Cabot (Unit 345, see [36]) that has been deployed  
221 in the central North Sea during 08/05/2018 - 15/08/2018 as a part of the  
222 Alternative Framework to Assess Marine Ecosystem Functioning in Shelf  
223 Seas (AlterECO) programme (<https://altereco.ac.uk/>). The satellite SST  
224 was bias-corrected following the scheme from [61], using the VIIRS and in  
225 situ SST data as the reference.

226 In the biogeochemical data assimilation we have included total log-chlorophyll  
227 derived from the ocean color based satellite product of ESA (version 2.0, [62])  
228 and also log-chlorophyll derived from the fluorescence measurements by the  
229 same AlterEco glider Cabot, that was used in the physical data assimilation.  
230 The assimilation is performed for log-chlorophyll, rather than chlorophyll, as  
231 chlorophyll is widely known to be log-normally distributed ([63]).

232 The assimilated in situ (EN4, glider) observations were thinned to a res-  
233 olution of  $0.08^\circ$  (EN4), or up-scaled to the AMM7 grid (glider), with addi-  
234 tional temporal averaging applied to the same-day glider observations. The  
235 thinning/up-scaling is performed to avoid assimilating many observations  
236 at higher resolution than the model can represent. After the thinning/up-  
237 scaling there were  $O(10^5)$  EN4 and  $O(10^4)$  Cabot glider data-points to as-  
238 simulate throughout the year 2018.

239 *2.3.2. Validation data*

240 The assimilated observations were used for the validation of those exper-  
241 iments in which they were excluded from the assimilation (e.g. chlorophyll  
242 data for the physical data assimilative run). However, we excluded the bias-  
243 corrected satellite SST from the temperature validation, so that the only  
244 assimilated SST data used for validation were a) the high quality SST data  
245 from the VIIRS satellite product and from ships, drifters and moorings (we  
246 will call this “VIIRS/in situ SST data”), and the SST that was part of b) EN4

247 and c) Cabot glider data. Besides the assimilated observations, all the exper-  
248 iments were validated with other (non-assimilated) AlterEco glider data for  
249 temperature, salinity, chlorophyll, oxygen and the sum of nitrate and nitrite  
250 (all the gliders included in the validation are listed in Tab.1). The processing  
251 of the physical, chlorophyll and oxygen data was described in [36]. The sum  
252 of nitrate and nitrite concentrations (abbreviated as  $\text{NO}_x^- = \text{NO}_3^- + \text{NO}_2^-$ )  
253 were determined using a Lab-on-Chip (LoC) analyser designed and fabricated  
254 at the National Oceanography Centre ([64]), which were implemented by the  
255 AlterEco team into Seagliders following a similar protocol as used by [65].  
256 The combined uncertainty (random and systematic errors) of measurements  
257 made using these LoC analysers has been calculated as  $\pm 5\%$  (coverage interval  
258  $k = 1$ ) ([66]). The nitrite concentrations were relatively negligible compared  
259 to the nitrate concentrations, so the  $\text{NO}_x^-$  data were used to validate model  
260 nitrate outputs. All of the used AlterEco gliders operated during 2018 in  
261 the central North Sea (for both the glider and the EN4 data locations see  
262 Fig.S1 of the Supporting Information (SI)), moving throughout the whole  
263 water column. Similar to the assimilated Cabot glider, the remaining glider  
264 data were up-scaled onto the model grid (on a daily basis) and after the up-  
265 scaling there remained  $O(10^4)$  AlterEco glider observations for each variable  
266 in 2018.

267 The EN4 data-set contained subsurface observations that were approxi-  
268 mately homogeneously distributed both with depth and in time, with slightly  
269 lower number of observations towards the end of the year (November-December  
270 2018). Beyond the assimilated data and the AlterEco data, we used for vali-  
271 dation a 1960-2014 monthly climatological dataset for total chlorophyll, oxy-  
272 gen, nitrate, phosphate and silicate concentrations, compiled in the North  
273 Sea Biogeochemical Climatology (NSBC) project ([67]). The NSBC dataset  
274 covers most of the NWE Shelf and the full range of depths. Finally, we also  
275 included validation of surface  $\text{CO}_2$  fugacity using 2018 SOCAT (v2019) data  
276 (<https://www.socat.info/index.php/about/>).

#### 277 2.4. The assimilative system: NEMOVAR

278 NEMOVAR is a variational (in this study a 3DVar) DA system ([68, 69,  
279 70]) used at the Met Office for operational reanalyses and forecasting on  
280 the NWE Shelf. The assimilation of ocean color-derived chlorophyll using  
281 NEMOVAR is highly successful in improving the NWE Shelf phytoplankton  
282 phenology, PFT community structure (using PFT chlorophyll assimilation),  
283 underwater irradiance and to a more limited degree also carbon cycle ([46, 31,

Table 1: The AlterEco gliders and the variables measured by the gliders used for assimilation (6-th column), or validation (7-th column). The table uses the following abbreviations: deployment:“dpl”, data assimilation:“DA”, temperature:“T”, salinity:“S”, oxygen concentrations:“O<sub>2</sub>”, chlorophyll *a* concentrations:“Chl *a*” and sum of nitrate and nitrite concentrations:“NO<sub>x</sub>-”.

Campaign	platform	dpl	serial	mission period	DA	validation
AlterEco 1	Stella	440	unit_436	02/02/2018 - 08/05/2018	none	T,S,O <sub>2</sub> ,Chl <i>a</i>
AlterEco 1	Cook	441	unit_194	15/11/2017 - 07/02/2018	none	T,S,O <sub>2</sub> ,Chl <i>a</i> ,NO <sub>x</sub> -
AlterEco 2	Orca	493	SG510	07/03/2018 - 27/03/2018	none	Chl <i>a</i> ,NO <sub>x</sub> -
AlterEco 2	Melonhead	496	SG620	07/02/2018 - 02/04/2018	none	Chl <i>a</i>
AlterEco 3	Cabot	454	unit_345	08/05/2018 - 15/08/2018	T,S,Chl <i>a</i>	T,S,O <sub>2</sub> ,Chl <i>a</i>
AlterEco 3	Orca	455	SG510	16/03/2018 - 24/07/2018	none	Chl <i>a</i> ,NO <sub>x</sub> -
AlterEco 3	Humpback	497	SG579	09/05/2018 - 25/06/2018	none	Chl <i>a</i>
AlterEco 4	Dolomite	477	unit_305	13/08/2018 - 10/10/2018	none	T,S,Chl <i>a</i> ,NO <sub>x</sub> -
AlterEco 4	Eltanin	478	SG550	15/08/2018 - 28/09/2018	none	Chl <i>a</i>
Altereco 5	Kelvin	481	unit_444	26/09/2018 - 02/12/2018	none	T,S,Chl <i>a</i>
AlterEco 6	Dolomite	499	unit_305	02/12/2018 - 12/03/2018	none	T,S,O <sub>2</sub> ,Chl <i>a</i>
AlterEco 6	Coprolite	500	unit_331	02/12/2018 - 12/03/2018	none	T,S,O <sub>2</sub> ,Chl <i>a</i>

71]). NEMOVAR includes capability to assimilate multi-platform (satellite, in situ) data, which has been established first for physics (e.g. [70, 72]) and subsequently for biogeochemistry ([73]), including validating the multi-platform DA system for the NWE Shelf ([36]).

The NEMOVAR set-up used in this study for the multi-platform physical-biogeochemical assimilation is the same as the one described in detail by [36]. Here we offer only a short summary: The 3DVar version of NEMOVAR uses a First Guess at Appropriate Time (FGAT) to calculate a daily set of increments for the directly updated variables ([70, 72]). In the physical DA application NEMOVAR applies balancing relationships within the assimilation step and delivers a set of increments for temperature, salinity, sea surface height (SSH) and the horizontal velocity components. For the total chlorophyll assimilation NEMOVAR calculates a set of log-chlorophyll increments and then a balancing scheme is used to distribute those increments into the PFT components (chlorophyll, carbon, nitrogen, phosphorus and for diatoms also silicon), all of which are being updated based on the background community structure and stoichiometric ratios (e.g. [46, 31, 36]). After the assimilation step, the model is re-run with the increments applied to the model variables gradually at each model time-step using incremental analysis updates (IAU, [74]).

304 NEMOVAR uses externally supplied spatio-temporally varying observa-  
 305 tion and background error variances, with the background error variances  
 306 typically 1-3 times larger than the observational error variances ([36]). The  
 307 system combines two horizontal correlation length-scales, one fixed 100km  
 308 length-scale with another length-scale based on the baroclinic Rossby radius  
 309 of deformation ([72]). The vertical length-scales follow the scheme from [72],  
 310 where NEMOVAR calculates directly the set of 3D increments using flow-  
 311 dependent vertical length-scales ( $\ell$ ), which are at the surface equal to half  
 312 of the MLD, decreasing in the mixed layer to become two-times the vertical  
 313 model grid spacing at, and beneath the MLD.

### 314 2.5. The experiments

315 In this study we compared the performance of both one-way and two-way  
 316 coupled versions of the NEMO-FABM-ERSEM model. We also tested the  
 317 impact of assimilating different types of data (physical-only, biogeochemical-  
 318 only and physical and biogeochemical jointly) on the skill of both the one-  
 319 way and two-way coupled models. The various experiments used exactly the  
 320 same model configuration, apart from the difference in the coupling between  
 321 physics and biogeochemistry. The experiments all started from the same  
 322 initial value conditions on the 01/09/2017 to allow a 4 month spin-up time for  
 323 the final 2018 simulation. The initial values were provided by the 2016-2018  
 324 free simulation (using bio-optical module) from the study of [31]. Finally,  
 325 Tab.2 provides a list of all experiments with their abbreviated names that  
 326 we will use in the paper.

### 327 2.6. Skill metrics

328 The performance of the different simulations will be evaluated using two  
 329 skill metrics. The first metric is the model bias ( $\Delta Q_{mo}$ ):

$$\Delta Q_{mo} = \langle Q_m - Q_o \rangle \quad (1)$$

330 where  $Q_o$  are the observations mapped into the model grid and the  $Q_m$  are  
 331 the corresponding model outputs. The second metric is the bias-corrected  
 332 root mean square difference (BC RMSD,  $\Delta_{RD}Q_{mo}$ ):

$$\Delta_{RD}Q_{mo} = \sqrt{\langle (Q_m - Q_o - \Delta Q_{mo})^2 \rangle}. \quad (2)$$

Table 2: The different experiments compared in this study. The first column shows the abbreviated experiment name, the second column indicates whether the two-way coupling is used and the following columns list the assimilated data. The table uses the following abbreviations: satellite:“sat”, Cabot glider:“Cabot”, EN4 dataset:“EN4”, temperature:“T”, sea surface temperature:“SST”, salinity:“S”, chlorophyll *a*:“Chl *a*”.

abbreviation	two-way	SST (sat./in situ)	T & S (EN4)	T & S (Cabot)	Chl <i>a</i> (sat.)	Chl <i>a</i> (Cabot)
free 1-way	no	no	no	no	no	no
free 2-way	yes	no	no	no	no	no
phys DA 1-way	no	yes	yes	yes	no	no
phys DA 2-way	yes	yes	yes	yes	no	no
chl DA 1-way	no	no	no	no	yes	yes
chl DA 2-way	yes	no	no	no	yes	yes
phys+chl DA 1-way	no	yes	yes	yes	yes	yes
phys+chl DA 2-way	yes	yes	yes	yes	yes	yes

### 333 3. Results and Discussion

#### 334 3.1. The impact of the two-way coupling and assimilation on the simulated 335 physics

336 The reference one-way coupled model simulates well the seasonal increase  
337 of temperature in the surface ocean in late-spring / summer (Fig.2:A, Fig.3).  
338 The novel two-way coupling further increased the temperature in the upper  
339 20m by around 1°C (Fig.2:B, Fig.3). This is a relatively major change with  
340 respect to the reference run, when compared to the changes introduced to  
341 the simulated temperature by the physical data assimilation during the same  
342 period of the year (Fig.2:D, for all the assimilative runs see Fig.S2-S3 in the  
343 Supporting Information (SI)). The increase in the upper ocean temperature  
344 in the two-way coupled model cannot be explained by the enhanced shortwave  
345 radiation flux in the water column, since the bio-optical module and the  
346 ERA5 short-wave radiation product, which forces the one-way coupled run,  
347 have a negligible mutual bias ([31]). Therefore, the temperature increase  
348 is likely a consequence of an increased rate of absorption inside the upper  
349 oceanic layer. The increased absorption in the two-way coupled run was  
350 anticipated since: a) the bio-optical module appears to have higher level of  
351 light attenuation near the water surface than the satellite observations used  
352 to force the physics in the one-way coupled run (this was observed for 490nm  
353 wavelength in Fig.5:A of [31]), b) the “broadband” visible light attenuation  
354 in the one-way coupled run was represented by the satellite  $K_d$  for 490nm

355 wavelength, but  $K_d$  at 490nm wavelength is clearly an underestimate of the  
356  $K_d$  for the 400-700nm waveband (see Fig.5:B of [31]).

357 The impact of phytoplankton biomass on the simulated temperature can  
358 be analysed by comparing the chlorophyll-assimilative run (chl DA 2-way)  
359 with its corresponding two-way coupled free run (free 2-way): In the late  
360 spring - summer, the assimilation of chlorophyll into the two-way coupled  
361 model removes a large amount of phytoplankton biomass from the mixed  
362 layer (see Fig.S4:B of SI), increases the light penetration into the water col-  
363 umn and heats up a deeper oceanic layer than the free run (Fig.2:B-C). The  
364 temperature is then raised in the 20-60m depth range by 0.1-0.2°C in the  
365 summer and by less than that in the late spring (see Fig.S5 of SI). The extra  
366 heat captured by the two-way coupled model near the ocean surface shallows  
367 the MLD (Fig.4:B, Fig.S6 of SI), which is indicative of important changes to  
368 mixing of biogeochemical tracers in the upper ocean.

369 Outside of the late spring - summer, both two-way coupling (Fig.2:B) and  
370 chlorophyll assimilation (Fig.2:C) have comparably smaller impact on the  
371 simulated oceanic temperature than the physical data assimilation (Fig.2:D,  
372 see also Fig.S2-S4 of SI). The impact of physical data assimilation is most  
373 important around the winter, when it corrects a negative temperature bias  
374 ( $\sim -0.5^\circ\text{C}$ ) of the physical model (Fig.2-3, Fig.S3-S4 of SI). The physical  
375 data assimilation influences the simulated temperature more evenly across  
376 the water column than the bio-optical module (Fig.2), which is likely a com-  
377 bination of model dynamical response to the temperature increments in the  
378 mixed layer and some assimilated sub-surface data (EN4 and Cabot glider).  
379 If the reanalysis state is sufficiently stable with respect to the model dynam-  
380 ics, it is known ([46, 31, 36]) that, within NEMOVAR on the NWE Shelf,  
381 the assimilated variables in the reanalysis tend to converge to the assimi-  
382 lated data. This is evident in the Fig.5:D, Fig.S3,S7 of SI, comparing the  
383 SST of the physical data assimilation runs with the assimilated satellite SST  
384 observations.

385 We evaluated (Fig.6 and Fig.7) the skill of both the two-way coupled  
386 model and the different assimilative experiments to represent temperature  
387 and salinity on the NWE Shelf. Fig.6 compares the two-way coupled free and  
388 chlorophyll-assimilative runs with the temperature and salinity measured by  
389 the Cabot glider mission in the central North Sea during late spring - summer  
390 of 2018 (for more details about the mission see [36], Fig.S1 of SI and Tab.1).  
391 Glider-observed temperature is warmer in the upper 30-40m of the water col-  
392 umn than the temperature simulated by the one-way coupled model, whereas

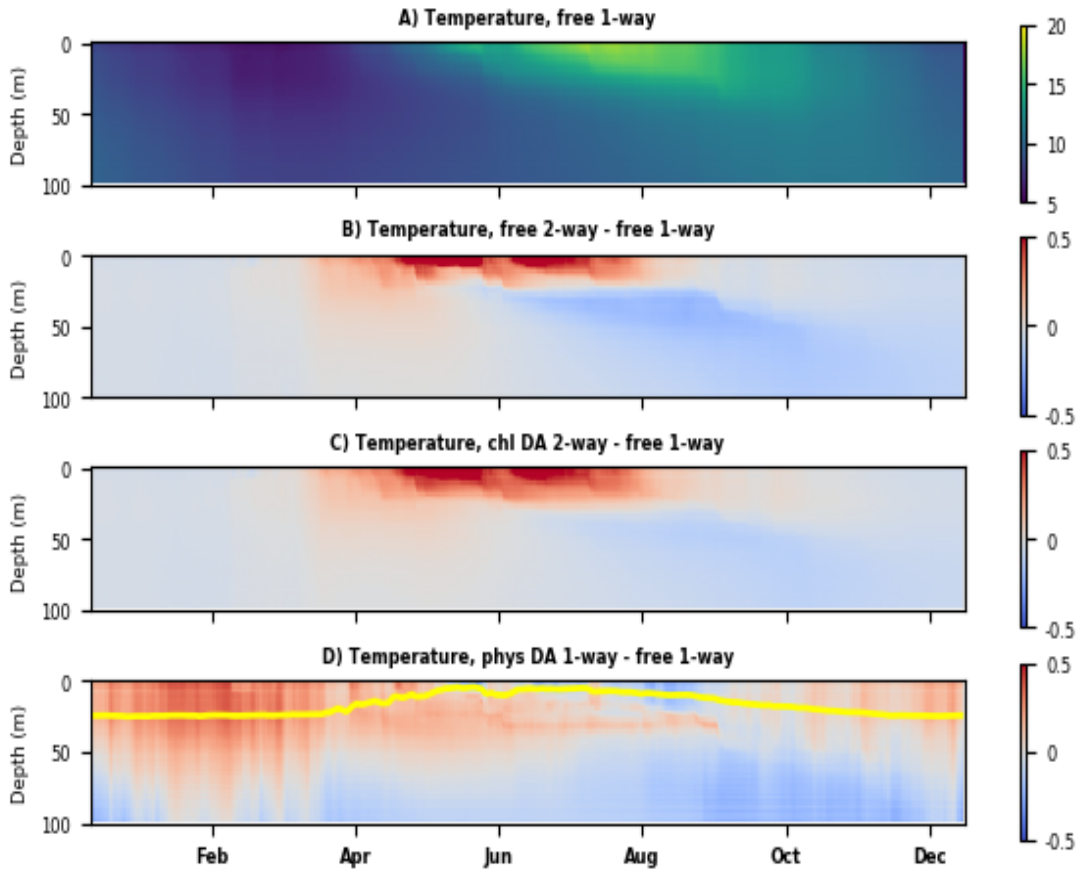


Figure 2: Panel A shows Hovmöller diagram (time on the x-axis vs depth on the y-axis) for the temperature ( $^{\circ}\text{C}$ ) of the one-way coupled free run, where the values for each day and depth represent the horizontal spatial averages throughout the NWE Shelf (bathymetry  $< 200\text{m}$ ). Panels B-D show the same Hovmöller diagrams as panel A, but for the temperature differences between the two-way coupled, or assimilative runs and the reference, free one-way coupled model run from the panel A (for the abbreviations used in the titles see Tab.2). In particular, panels B-D compare the impact of two-way coupling on the simulated temperature (panel B), joint impact of chlorophyll-assimilation and two-way coupling on the simulated temperature (panel C) and the impact of physical data assimilation on the simulated temperature (panel D). The yellow line in the panel D shows the MLD of the physical data assimilative run to indicate the vertical scale of impact of the SST assimilation.

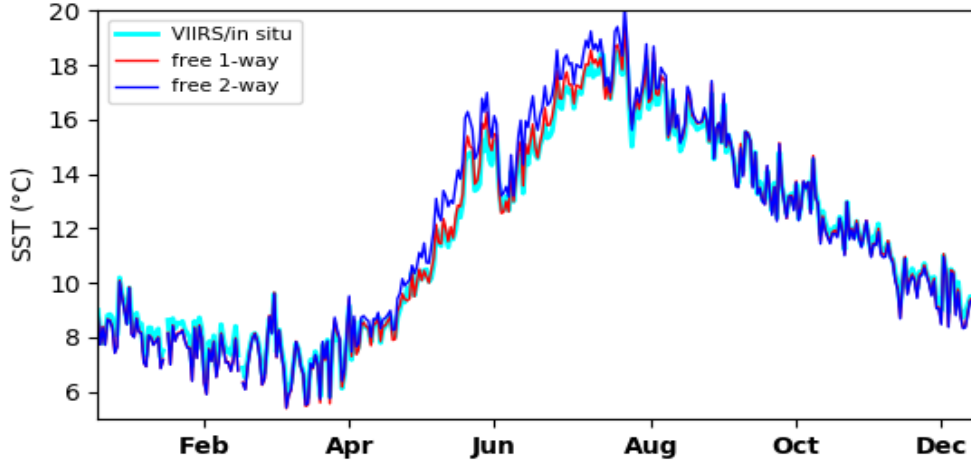


Figure 3: The 2018 time-series of SST averaged throughout the NWE Shelf compared between the one-way and two-way coupled free simulations, and the VIIRS satellite/in situ data. To consistently compare the model simulations with the observed SST, the model outputs were masked wherever there were missing observations. The missing satellite observations are due to the movements of clouds and atmospheric disturbances and the missing values are responsible for the small time-scale fluctuations in the different curves shown in the plot.

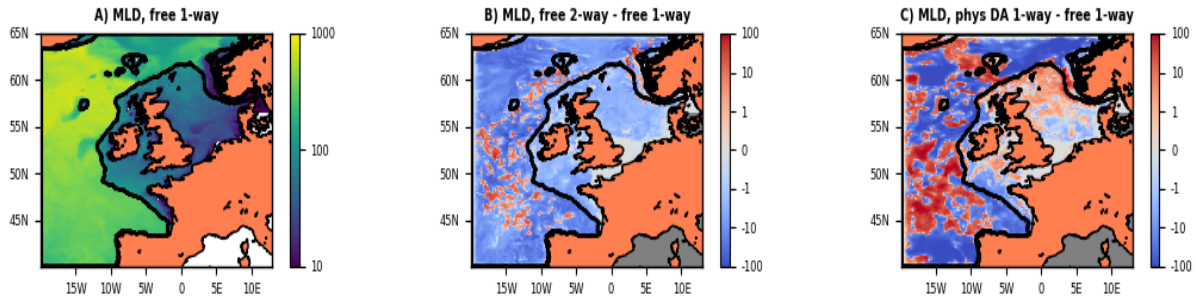


Figure 4: Panel A shows the mixed layer depth (MLD, in m) of the one-way coupled reference free run. The MLD values are averaged for the spring bloom period between March-May 2018. Panels B-C show the relative changes in MLD carried by the two-way coupled free run (panel B) and physical data assimilation into the one-way coupled model (panel C). Both panels B,C show the difference (in m) between the MLD of the two-way coupled, or physical data assimilative run and the one-way coupled model free run (panel A). The blue color in panels B-C (negative values) indicates shallowing of MLD, whilst the red color (positive values) indicates deepening of MLD. The black line shows the boundary of the continental shelf (bathymetry < 200m).

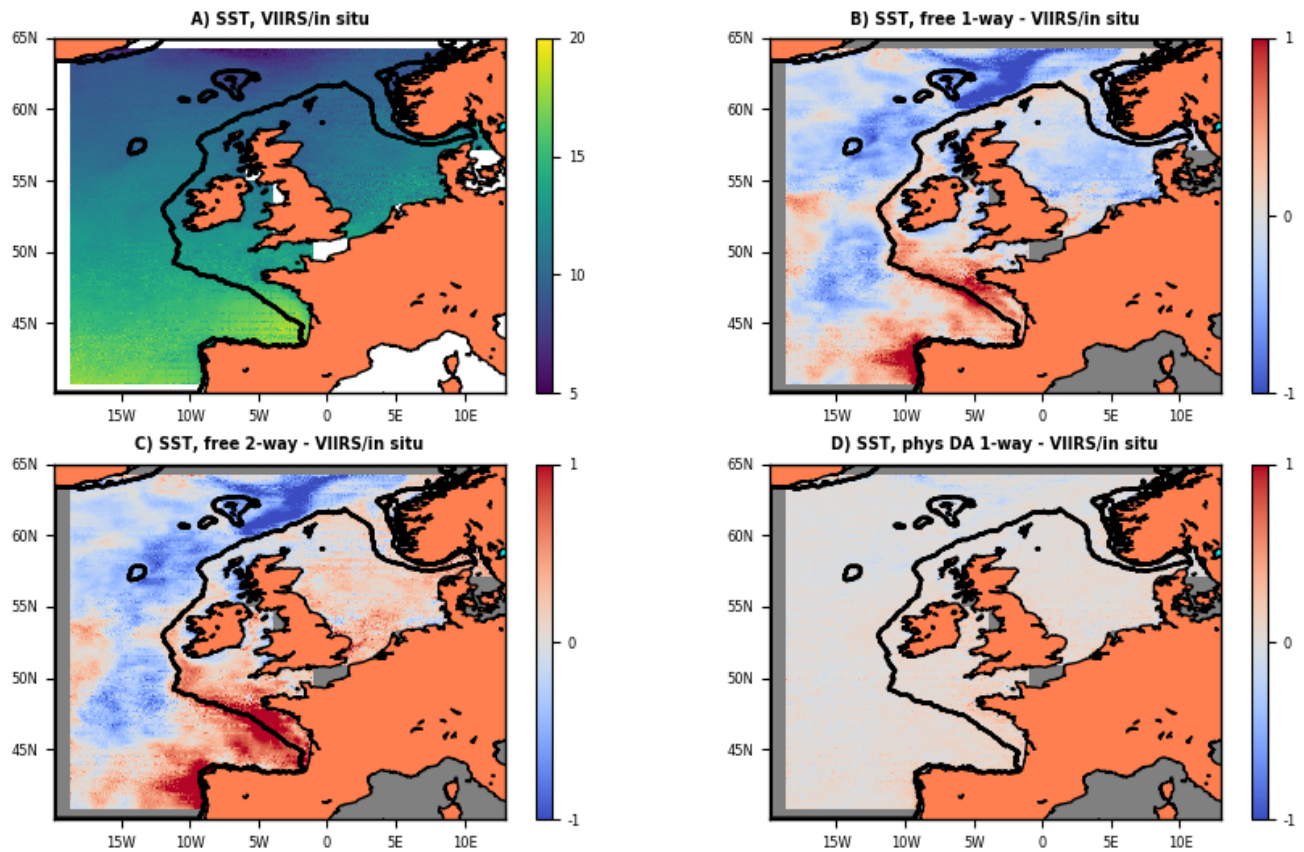


Figure 5: The assimilated 2018 median satellite data for SST (panel A, in °C) and the corresponding model to VIIRS/in situ SST differences (panels B-D, in °C) for one-way coupled model free run (panel B), two-way coupled model free run (panel C) and physical data assimilation into the one-way coupled free run (panel D). The masked values indicate the regions where there was no assimilation of VIIRS/in situ data into the model.

393 the opposite is true beneath 40m depth (Fig.6:A). This means the observed  
394 thermocline represents a larger gradient in temperature than the simulated  
395 thermocline. The bio-optical module substantially (by  $> 1^{\circ}\text{C}$ ) heats up the  
396 upper 20-30m layer, increasing the vertical temperature gradient (Fig.6:C),  
397 however the near-surface temperature of the two-way coupled run rises well  
398 above the levels observed by the glider (Fig.6:D). The thermocline of the  
399 two-way coupled model free run appears to be located above the glider ther-  
400 mocline (e.g. Fig.6:D) and the impact of the two-way coupling on the model  
401 skill in representing glider temperature is somewhat mixed (it improves bias,  
402 but degrades BC RMSD, Fig.7:A). The skill validation presented in Fig.7  
403 shows similarly mixed results: the summer temperature bias is improved  
404 across the EN4 and AlterEco glider data, but degraded relative to the VI-  
405 IRS/in situ data (see also Fig.3), with the BC RMSD consistently degraded  
406 across the different validation data. The Fig.7:A indicates that the two-  
407 way coupling produces better results for sub-surface summer temperature,  
408 than for SST (VIIRS/in situ data). The two-way coupling has a similarly  
409 mixed impact on the free run skill to represent summer salinity (Fig.7:C),  
410 and both small ( $< 0.05^{\circ}\text{C}$ ) and mixed impact on winter temperature and  
411 salinity (Fig.7:B,D, for temperature see also Fig.2-3). However, it should be  
412 noted that chlorophyll assimilation into the two-way coupled model slightly  
413 improves the skill of the free run in representing temperature and salinity  
414 across most of the data and throughout the whole year 2018 (Fig.7). Finally,  
415 the comparison with the non-assimilated temperature validation data clearly  
416 demonstrates that the physical data assimilation improves the model skill in  
417 temperature both in summer and winter half-year (Fig.7:A-B) and also the  
418 model skill in salinity in the winter half-year (Fig.7:D).

### 419 *3.2. The impact of the two-way coupling and assimilation on biogeochemistry*

420 As the days in spring become longer, the layer that is effectively lit by  
421 the sunlight expands into the water column, whilst the effective mixing depth  
422 shrinks. It is often assumed, that the effective mixing depth reaching a critical  
423 threshold marks the onset of the spring bloom (Fig.1). This process might be  
424 misrepresented by the one-way coupled reference free simulation, which could  
425 be why the model shows on the NWE Shelf late (by  $\sim 1$  month) and intense  
426 blooms (Fig.8, see also [31, 36]). The effective mixing depth has often been  
427 interpreted as the seasonal MLD (this is the frequent understanding of the  
428 critical depth hypothesis of [75]), but it is assumed that on the NWE Shelf  
429 the onset of the bloom might be better described by the critical turbulence

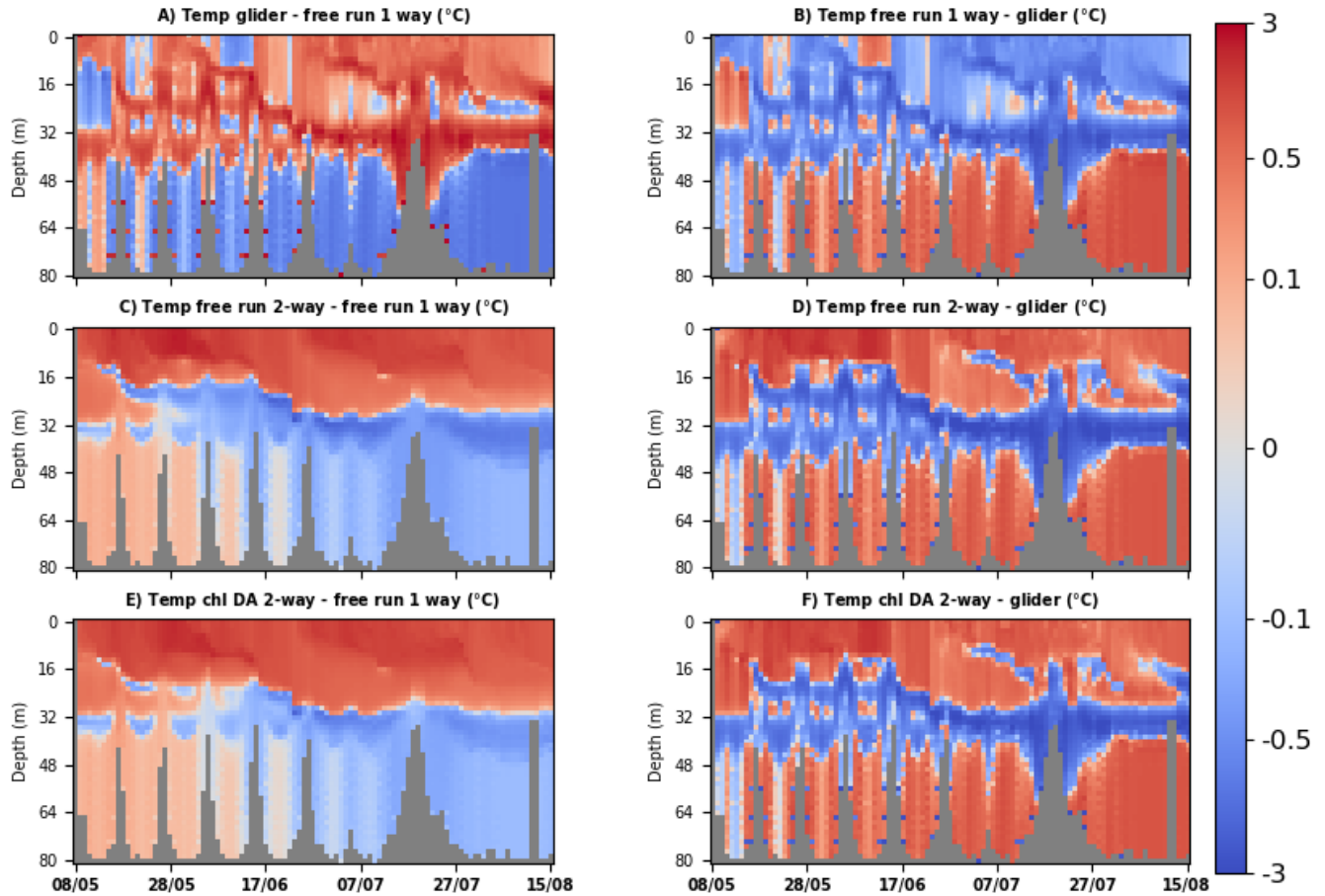


Figure 6: Hovmöller diagram for temperature ( $^{\circ}\text{C}$ ) along the trajectory covered by the Cabot glider in the central North Sea during an early May to mid-August 2018 mission. The right-hand panels (B,D,F) show the temperature differences between the free one-way coupled run (panel B), free two-way coupled run (panel D), the chlorophyll assimilation into the two-way coupled model (panel F) and the Cabot glider observations (model minus glider). The left hand panels (A,C,E) show the differences between the observations, or model simulations and the reference, free one-way coupled model run. The purpose of the left-hand panels is to show the desired changes to the one-way coupled model (panel A) and how these changes are realized by the biogeochemical feedback in the free run (panel C) and in the chlorophyll-assimilative run (panel E). The main advantage of those left-hand (A,C,E) panels is that they allow relatively easy interpretation of the dynamical changes introduced to the reference run by the biogeochemical feedback to physics and/or data assimilation.

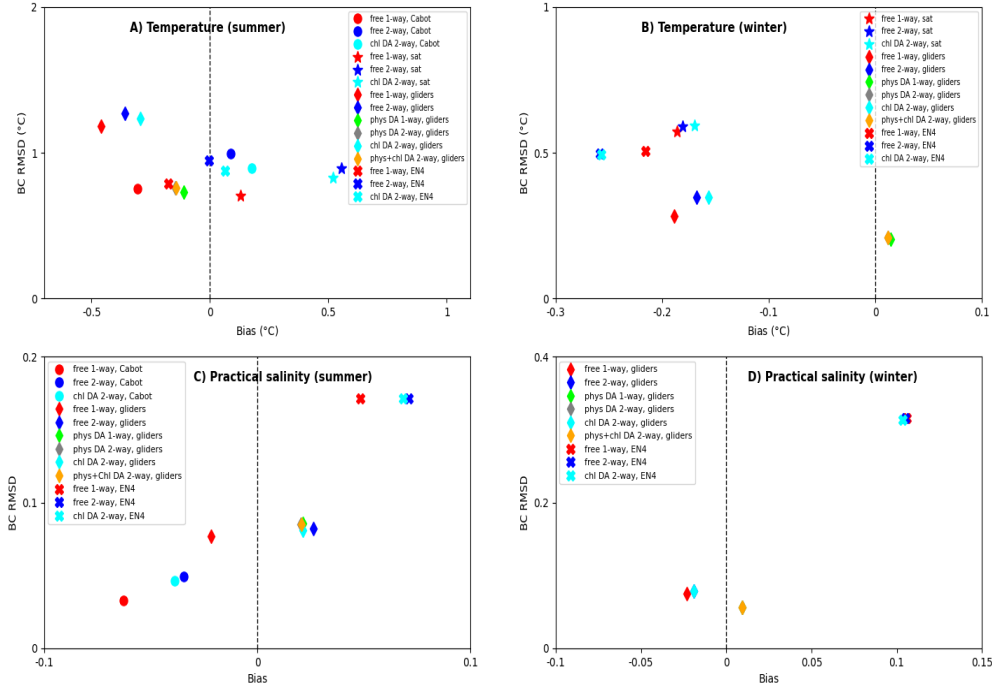


Figure 7: Skill of the different model simulations to represent temperature ( $^{\circ}\text{C}$ , panels A-B) and practical salinity (panels C-D). The skill is measured by bias (x-axis, Eq.1) and BC RMSD (y-axis, Eq.2). The skill is evaluated for two half-year periods of 2018, the “summer” (panels A,C) defined as May-October and the “winter” (panels B,D) defined as November-April (data averaged through January-April 2018 and November-December 2018). The different simulations are represented by different colors: free run of the one-way coupled model (red), free run of the two-way coupled model (blue), assimilation of chlorophyll into the two-way coupled model (cyan), physical data assimilation into the one-way coupled model (lime), physical data assimilation into the two-way coupled model (grey) and joint physical data-chlorophyll assimilation into the two-way coupled model (orange). The different markers show comparison with different data-sets: the star stands for the VIIRS/in situ SST, the circle for the Cabot glider observations, the diamond for the remaining available glider observations (the 2018 AlterEco mission without Cabot) and the cross for the EN4 data-set. The data (SST, Cabot, EN4) which were assimilated in some of the simulations were used to validate only the simulations that avoided their assimilation.

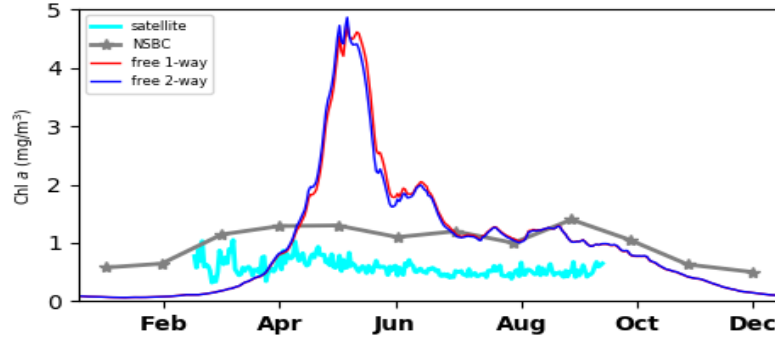


Figure 8: The 2018 time-series of surface chlorophyll  $a$  concentrations ( $\text{mg}/\text{m}^3$ ) averaged throughout the NWE Shelf compared between the one-way and two-way coupled free simulations, the satellite data, as well as with the NSBC climatological data-set. The satellite data were considered only in the March-September period as the data outside this period are scarce and limited only to the southern part of the NWE domain. The small time-scale fluctuations in the satellite data are due to the missing values caused by the movement of clouds and atmospheric disturbances.

430 hypothesis ([40]). In the critical turbulence hypothesis the bloom starts when  
 431 the turbulent mixing in the upper ocean drops beneath a critical level, whilst  
 432 the effective rate of turbulent mixing is largely decoupled from the seasonal  
 433 MLD ([40, 41, 42]).

434 The implementation of the bio-optical module was shown to shallow the  
 435 MLD (Fig.4), but it can also reduce convection within the mixed layer and  
 436 the turbulent mixing. The starting hypothesis of this work was that the extra  
 437 heat captured in the upper oceanic layer could trigger an earlier bloom  
 438 and improve the ERSEM skill. Fig.8, Fig.9:B and Fig.10:C-D show that the  
 439 changes to the simulated physics introduced through the two-way coupled  
 440 model indeed trigger an earlier phytoplankton bloom, but the difference in  
 441 the bloom timing is only on the scale of several days, rather than weeks.  
 442 However, the shift to the bloom timing has an impact on many subsequent  
 443 features, such as the deep chlorophyll maxima (e.g. [36]), so the changes  
 444 to the bloom onset can gradually propagate to the subsurface chlorophyll  
 445 (Fig.9:C). The model skill to simulate chlorophyll is improved by the two-  
 446 way coupling quite notably in the central North Sea and the period covered  
 447 by the Cabot glider (Fig.11:A), however comparisons with other data spread  
 448 throughout the year 2018 (satellite ocean color, remaining AlterEco gliders  
 449 and the NSBC climatology) show only small improvement (Fig.11:A). The

450 modest improvement to the timing of the (delayed) spring bloom through  
451 the changed mixing is certainly a disappointment, and we suspect that to  
452 introduce a larger correction to the timing of the bloom it would be nec-  
453 essary to either improve the physical model mixing scheme, or to improve  
454 some key ERSEM parameters and processes, such as P-I curves, the max-  
455 imum chlorophyll-to-carbon ratios, zooplankton grazing and representation  
456 of plankton mixotrophy ([29]).

457 Although the (modest) improvements to the simulated chlorophyll by the  
458 two-way coupled model originate from its changes to the simulated physics  
459 (i.e. vertical mixing), the physical data assimilation, which substantially im-  
460 proves the simulated physics (Fig.7) does not improve (even slightly degrades)  
461 the model skill in chlorophyll (Fig.11:A). This is likely because the physical  
462 data assimilation is for large part the assimilation of SST. The improvement  
463 in the ecosystem model skill depends mostly on the vertical mixing and lim-  
464 ited changes to vertical mixing are expected by assimilating SST. Assimilated  
465 subsurface temperature and salinity data are quite sparse, and have only a  
466 limited impact on the modelled biogeochemistry. In the case of the Cabot  
467 glider “case-study” presented in Fig.10 (for a more complete view see Fig.S8  
468 of SI), the glider temperature and salinity assimilation did not improve the  
469 simulated chlorophyll at the glider locations (Fig.11:A) mostly because the  
470 impact of physics on biogeochemistry needs some spin-up time. In fact in  
471 the last part of the glider mission period (late July-August in Fig.10:E) the  
472 physical assimilation has some potential to improve the chlorophyll concen-  
473 trations, as was demonstrated by the assimilation of the same Cabot glider  
474 data in Fig.6E of [36]. Finally, the chlorophyll assimilation dominates over  
475 both physical assimilation and two-way coupling in its impact on the simu-  
476 lated chlorophyll concentrations across the whole water column and the whole  
477 simulation year (Fig.9:D and Fig.S9 of SI). Since the chlorophyll assimi-  
478 lation is almost entirely based on the satellite ocean color, chlorophyll beneath  
479 the mixed layer is updated through the model dynamical response to the  
480 assimilation (e.g. vertical mixing). Similarly to temperature, the chlorophyll  
481 reanalyses look very similar to the assimilated data (Fig.12:B-C, Fig.S5 and  
482 Fig.S10 of SI) and also validate much better than the free runs relative to  
483 the non-assimilated AlterEco glider data (Fig.11:A).

484 We validated the model simulation of additional biogeochemical variables  
485 with available observational data: oxygen, nitrate, phosphate, silicate and  
486 CO<sub>2</sub> fugacity. The oxygen concentrations are mostly driven by the primary  
487 productivity, respiration and outgassing, which largely depends on the sea

488 temperature. The two-way coupled model improves the model skill in repre-  
489 senting Cabot oxygen (Fig.11:B), which is likely triggered by the fact that the  
490 same simulation improves both Cabot chlorophyll (Fig.11:A) and the temper-  
491 ature bias (Fig.7:A). Equivalently, model skill in representing Cabot glider  
492 oxygen can be improved by assimilating physical data into the model (phys  
493 DA 1-way), and it is to some degree also improved by assimilating chloro-  
494 phyll (chl DA 1-way, chl DA 2-way), with the best performance achieved  
495 when both the physical data and chlorophyll are assimilated into the model  
496 (Fig.11:B). However, the Cabot glider study is specific, since the glider mis-  
497 sion took place in the period of the largest discrepancy in the simulated  
498 and observed productivity (Fig.8) and the oxygen concentrations were mea-  
499 sured by the same glider that provided temperature, salinity and chlorophyll  
500 data for assimilation. For the remaining non-assimilated AlterEco gliders  
501 the impact of two-way coupling and assimilation on simulated oxygen is less  
502 clear (Fig.11:B), i.e. even though AlterEco chlorophyll is improved by the  
503 chlorophyll-only assimilative runs (Fig.11:A) they mostly degrade simulated  
504 oxygen (Fig.11:B). This is likely due to the complex relationship between phy-  
505 toplankton chlorophyll and oxygen (see [36]), which includes respiration of  
506 oxygen by the higher trophic-level species (in ERSEM it is zooplankton and  
507 heterotrophic bacteria). However, improved representation of temperature  
508 consistently improves model oxygen bias across all the used data (Fig.11:A),  
509 which indicates that an important part of oxygen bias is due to model biases  
510 in temperature and not due to errors in the simulated biogeochemistry.

511 Besides oxygen, we looked at the model skill in how it represents the  
512 surface  $\text{CO}_2$  fugacity, which is influenced by the model skill in simulating  
513 primary productivity and sea temperature (gas solubility). Fig.11:C shows  
514 that  $\text{CO}_2$  fugacity is substantially improved by all the runs that included  
515 chlorophyll assimilation, which indicates that the assimilation of chlorophyll  
516 improved the phytoplankton carbon biomass and therefore the simulated  
517 carbon cycle (see also [46]). The physical data-only assimilative runs, and  
518 the two-way coupled free run, had more limited impact on the model skill  
519 to represent surface  $\text{CO}_2$  fugacity, but they sometimes reduced the model  
520 bias in  $\text{CO}_2$  fugacity. Both the two-way coupling and the physical assimi-  
521 lation, have a relatively small impact on the nitrate and phosphate concen-  
522 trations (Fig.11:D-E), however the changed phytoplankton biomass through  
523 the chlorophyll assimilation lowers the nitrate and phosphate concentrations  
524 at the NSBC data-set locations. This has a positive impact on the nitrate  
525 bias and a negative impact on the phosphate bias (Fig.11:D-E). Silicate is

526 impacted more by the physical data assimilation than nitrate and phosphate,  
527 but it is mostly degraded by all the assimilative runs (Fig.11:F).

#### 528 **4. Summary**

529 In this work we used a recently developed bio-optical module to improve  
530 the representation of oceanic heat fluxes and to introduce a biogeochemical  
531 feedback to the physical marine model (we call the model with such feedback  
532 “a two-way coupled model”). We have estimated the scale of the biogeochem-  
533 ical impact on the simulated physics and we have shown that in the upper  
534 oceanic layer, in the late spring - summer period, the feedback is comparable  
535 to the physical data assimilation in its impact on the simulated tempera-  
536 ture. The bio-optical module increases the heat captured in the upper part  
537 of the water column, steepens the vertical temperature gradient and shall-  
538 lows the mixed layer depth. We have shown that the changes introduced by  
539 the bio-optical module into the physical marine model have a mixed impact  
540 on the physical model skill. The skill is however (slightly) improved by the  
541 chlorophyll assimilation into the two-way coupled model and substantially  
542 improved by the physical data assimilation.

543 The increased stratification of the water column and the shallowed mixed  
544 layer depth have a modest positive impact on the timing of the late bloom  
545 displayed by the biogeochemical model. The shift in the timing of the bloom  
546 in the two-way coupled model improves the model skill in representing chloro-  
547 phyll. We conclude that, for a more substantial improvement of the timing  
548 of the bloom, it will be necessary to either improve the physical model mix-  
549 ing scheme, or to improve the process description, or parametrization of the  
550 biogeochemical model. We have expanded our analysis to include other bio-  
551 geochemical tracers, and we have found that the two-way coupled model and  
552 the physical data assimilation may sometimes help improve the agreement of  
553 simulated oxygen concentrations and  $\text{CO}_2$  fugacity with observations, both  
554 due to improved simulation of the sea water temperature (saturation levels)  
555 and productivity.

556 This study provides important evidence to support the inclusion of two-  
557 way coupling into future operational models of the NWE Shelf. Furthermore,  
558 the physical-biogeochemical assimilative runs on the NWE Shelf, including  
559 this work, are typically only weakly coupled (for one recent exception see  
560 [76]), in the sense that the physical and the biogeochemical variables are  
561 updated independently and interact only through the model dynamics. The

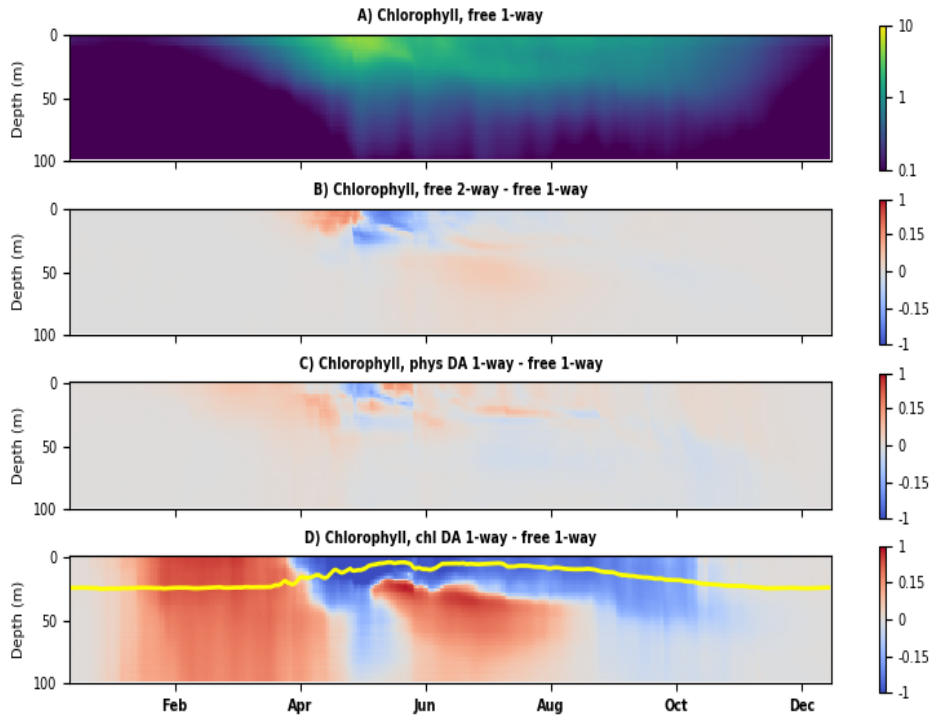


Figure 9: Impact of two-way coupling and assimilation on the simulated chlorophyll concentrations ( $\text{mg}/\text{m}^3$ ). Panel A shows Hovmöller diagram (time on the x-axis vs depth on the y-axis) for the one-way coupled model free run, where the values for each day and depth represent the horizontal spatial averages throughout the NWE Shelf (bathymetry  $< 200\text{m}$ ). Panels B-D show the same Hovmöller diagrams, but for the difference between the specific simulation and the reference, free one-way coupled run. The purpose of the panels B-D is to provide an understanding of how the two-way coupling (panel B), the biogeochemical feedback (panel C) and the chlorophyll-assimilation (panel D) influence the chlorophyll concentrations of the reference free one-way coupled run. The yellow line in the panel D shows the mixed layer depth, providing the boundary of the region in which the ocean color assimilation directly updates the simulated chlorophyll.

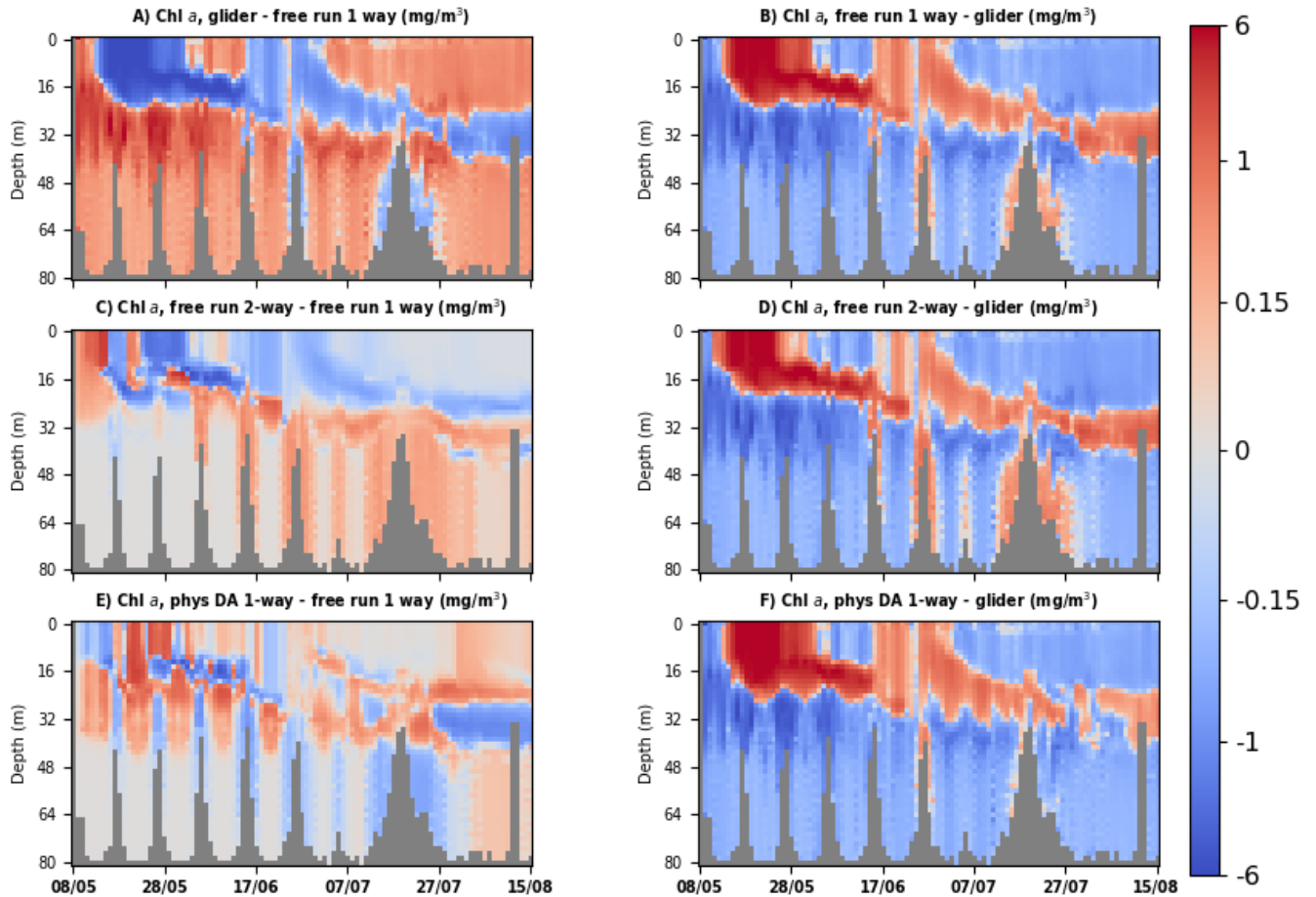


Figure 10: Hovmöller diagram for chlorophyll concentrations ( $\text{mg/m}^3$ ) along the Cabot glider trajectory in the central North Sea during an early May to mid-August 2018 mission. The right-hand panels (B,D,F) show the chlorophyll differences between the free one-way coupled model run (panel B), free two-way coupled model run (panel D), the physical data assimilation into the one-way coupled model (panel F), and the Cabot glider observations (model minus glider). The left hand panels (A,C,E) show the differences between the observations, or model simulations and the reference, free one-way coupled model run. The purpose of the left-hand panels is to show the desired changes to the one-way coupled model (panel A) and how these changes are realized by the biogeochemical feedback in the free run (panel C) and in the physical data-assimilative run (panel E). The main advantage of those left-hand panels is that they allow relatively easy interpretation of the dynamical changes introduced to the reference run by the biogeochemical feedback to physics and/or data assimilation.

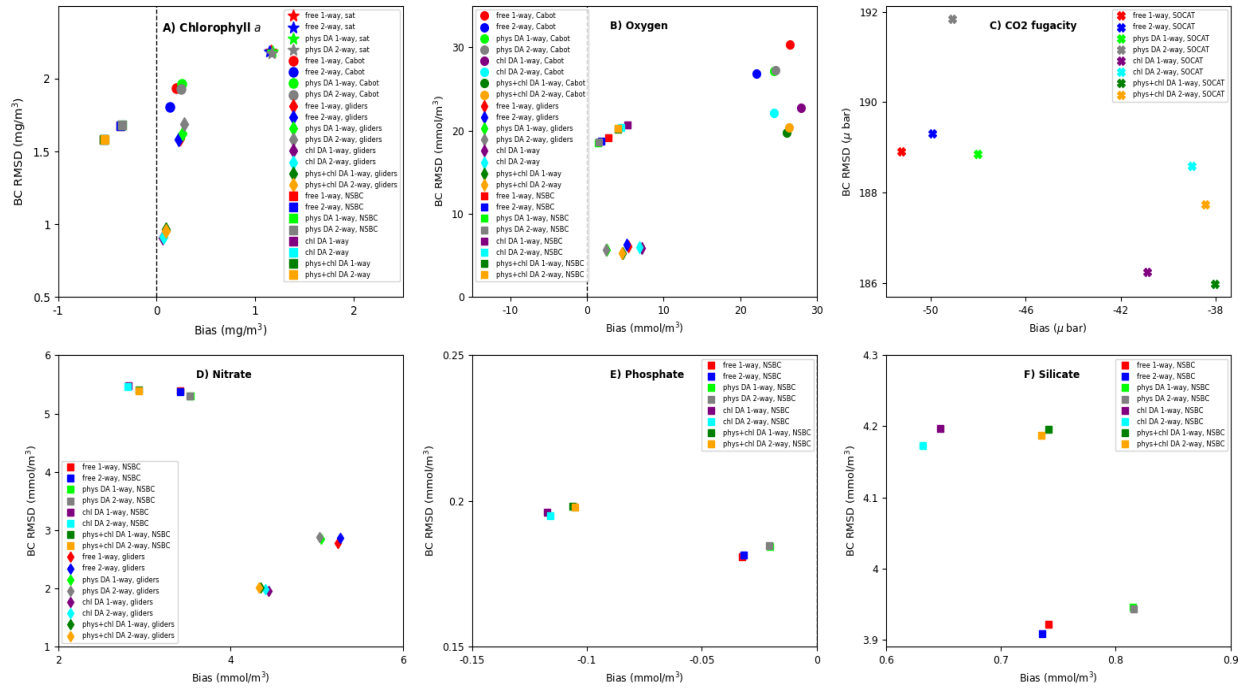


Figure 11: Skill of the different model simulations to represent chlorophyll *a* (mg/m<sup>3</sup>, panel A), oxygen (mmol/m<sup>3</sup>, panel B), CO<sub>2</sub> fugacity (μ bar, panel C), nitrate (mmol/m<sup>3</sup>, panel D), phosphate (mmol/m<sup>3</sup>, panel E) and silicate (mmol/m<sup>3</sup>, panel F) concentrations. The skill is measured by bias (x-axis, Eq.1) and BC RMSD (y-axis, Eq.2). The skill is evaluated for the full year 2018. The different simulations are represented by different colors: free run of the one-way coupled model (red), free run of the two-way coupled model (blue), assimilation of chlorophyll into the one-way coupled model (purple), assimilation of chlorophyll into the two-way coupled model (cyan), physical data assimilation into the one-way coupled model (lime), physical data assimilation into the two-way coupled model (grey), joint physical data-chlorophyll assimilation into the one-way coupled model (green) and joint physical data-chlorophyll assimilation into the two-way coupled model (orange). The different markers show comparison with different data-sets: the star stands for the satellite ocean color data, the circle for the Cabot glider observations, the diamond for the remaining available glider observations (the 2018 AlterEco mission without Cabot), the cross for the SOCAT data and the square for the NSBC climatological data-set.

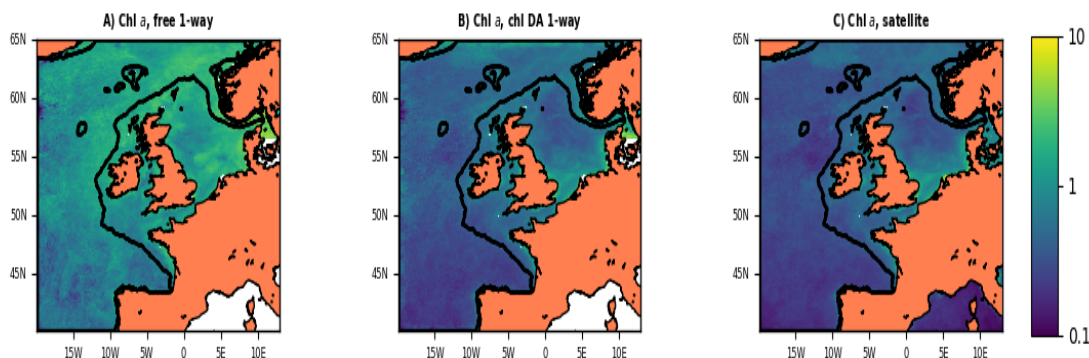


Figure 12: The 2018 mean surface chlorophyll concentrations (in  $\text{mg}/\text{m}^3$ ). The different panels compare: the one-way coupled model free run (panel A), the chlorophyll assimilation into the one-way coupled model free run (panel B), and the assimilated satellite ocean color observations (panel C). In the annual averaging we masked the model outputs wherever the satellite data were missing. The black line shows the continental shelf boundary (bathymetry  $< 200\text{m}$ ).

562 interaction between physics and biogeochemistry via the coupled model dy-  
 563 namics has been strengthened through the two-way coupling, but it would  
 564 be much more efficient if the assimilative updates to the physics and bio-  
 565 geochemistry interacted directly through their cross-covariances, or a bal-  
 566 ancing component within a data assimilation system. Such scheme is called  
 567 “strongly coupled”, and would provide the physical assimilation with both  
 568 faster and greater impact on the biogeochemical model skill, and vice versa.  
 569 Future work will use the two-way coupled model and expand the data assimi-  
 570 lation scheme to include such strong coupling into our operational system.

## 571 Acknowledgments

572 This work was supported by a Natural Environment Research Council  
 573 (NERC) funded project of the Marine Integrated Autonomous Observing  
 574 Systems (MIAOS) programme: Combining Autonomous observations and  
 575 Models for Predicting and Understanding Shelf seas (CAMPUS). It also ben-  
 576 efitting from another NERC funded project Alternative Framework to Assess  
 577 Marine Ecosystem Functioning in Shelf Seas (AlterECO, <http://projects.noc.ac.uk/altereco/>), grant no. NE/P013899/1. The work also benefited from  
 578 the Copernicus Marine Environment Monitoring Service (CMEMS) funded  
 579 projects OPTical data Modelling and Assimilation (OPTIMA) and NOWMAPS.  
 580

581 Furthermore, this work was also partially funded by the SEAMLESS project,  
582 which received funding from the European Union’s Horizon 2020 research  
583 and innovation programme under grant agreement No 101004032. We would  
584 like to thank Dawn Ashby for drawing the schematic Fig.1. The ocean color  
585 data were provided by the European Space Agency Climate Initiative “Ocean  
586 Color” (<https://esa-oceancolour-cci.org/>). The glider data used in the study  
587 (doi:10.5285/b57d215e-065f-7f81-e053-6c86abc01a82 and doi:10.5285/b58e83f0-  
588 d8f3-4a83-e053-6c86abc0bbb5) are publicly available on [https://www.bodc.ac.uk/-  
590 data/published\\_data\\_library/catalogue/](https://www.bodc.ac.uk/-<br/>589 data/published_data_library/catalogue/). The model was forced by the atmo-  
591 spheric ERA5 product of The European Centre for Medium-Range Weather  
592 Forecasts (ECMWF, <https://www.ecmwf.int/>). The river forcing data used  
593 by the model were prepared by Sonja van Leeuwen and Helen Powley as part  
594 of UK Shelf Seas Biogeochemistry programme (contract no. NE/K001876/1)  
595 of the NERC and the Department for Environment Food and Rural Affairs  
596 (DEFRA). We acknowledge use of the MONSooN system, a collaborative  
597 facility supplied under the Joint Weather and Climate Research Programme,  
598 a strategic partnership between the Met Office and the NERC. The differ-  
599 ent outputs for the free run simulations and reanalyses are stored on the  
MONSooN storage facility MASS and can be obtained upon request.

## 600 **References**

- 601 [1] M. Gehlen, R. Barciela, L. Bertino, P. Brasseur, M. Butenschön, F. Chai,  
602 A. Crise, Y. Drillet, D. Ford, D. Lavoie, et al., Building the capacity for  
603 forecasting marine biogeochemistry and ecosystems: recent advances  
604 and future developments, *Journal of Operational Oceanography* 8 (sup1)  
605 (2015) s168–s187.
- 606 [2] D. Ford, S. Kay, R. McEwan, I. Totterdell, M. Gehlen, Marine biogeo-  
607 chemical modelling and data assimilation for operational forecasting,  
608 reanalysis, and climate research, *New Frontiers in Operational Oceanog-  
609 raphy* (2018) 625–652.
- 610 [3] C. Heinze, M. Gehlen, Modeling ocean biogeochemical processes and  
611 the resulting tracer distributions, in: *International Geophysics*, Vol. 103,  
612 Elsevier, 2013, pp. 667–694.
- 613 [4] U. Riebesell, A. Körtzinger, A. Oschlies, Sensitivities of marine carbon

- 614 fluxes to ocean change, *Proceedings of the National Academy of Sciences*  
615 106 (49) (2009) 20602–20609.
- 616 [5] Z. Jin, T. P. Charlock, W. L. Smith Jr, K. Rutledge, A parameterization  
617 of ocean surface albedo, *Geophysical research letters* 31 (22) (2004).
- 618 [6] A. Morel, Optical modeling of the upper ocean in relation to its  
619 biogenous matter content (case i waters), *Journal of geophysical re-*  
620 *search: oceans* 93 (C9) (1988) 10749–10768.
- 621 [7] J.-y. Simonot, E. Dollinger, H. Le Treut, Thermodynamic-biological-  
622 optical coupling in the oceanic mixed layer, *Journal of Geophysical Re-*  
623 *search: Oceans* 93 (C7) (1988) 8193–8202.
- 624 [8] S. Sathyendranath, A. D. Gouveia, S. R. Shetye, P. Ravindran, T. Platt,  
625 Biological control of surface temperature in the arabian sea, *Nature*  
626 349 (6304) (1991) 54.
- 627 [9] A. M. Edwards, D. G. Wright, T. Platt, Biological heating effect of  
628 a band of phytoplankton, *Journal of Marine Systems* 49 (1-4) (2004)  
629 89–103.
- 630 [10] M. Manizza, C. Le Quéré, A. J. Watson, E. T. Buitenhuis, Bio-optical  
631 feedbacks among phytoplankton, upper ocean physics and sea-ice in a  
632 global model, *Geophysical Research Letters* 32 (5) (2005).
- 633 [11] C. Sweeney, A. Gnanadesikan, S. M. Griffies, M. J. Harrison, A. J.  
634 Rosati, B. L. Samuels, Impacts of shortwave penetration depth on large-  
635 scale ocean circulation and heat transport, *Journal of Physical Oceanog-*  
636 *raphy* 35 (6) (2005) 1103–1119.
- 637 [12] M. Lengaigne, C. Menkes, O. Aumont, T. Gorgues, L. Bopp, J.-M.  
638 André, G. Madec, Influence of the oceanic biology on the tropical pacific  
639 climate in a coupled general circulation model, *Climate Dynamics* 28 (5)  
640 (2007) 503–516.
- 641 [13] L. Zhai, C. Tang, T. Platt, S. Sathyendranath, Ocean response to at-  
642 tenuation of visible light by phytoplankton in the gulf of st. lawrence,  
643 *Journal of Marine Systems* 88 (2) (2011) 285–297.

- 644 [14] A. Turner, M. Joshi, E. Robertson, S. Woolnough, The effect of arabian  
645 sea optical properties on sst biases and the south asian summer monsoon  
646 in a coupled gcm, *Climate dynamics* 39 (3-4) (2012) 811–826.
- 647 [15] J. E. Lovelock, R. Maggs, R. Rasmussen, Atmospheric dimethyl sulphide  
648 and the natural sulphur cycle, *Nature* 237 (5356) (1972) 452–453.
- 649 [16] R. J. Charlson, J. E. Lovelock, M. O. Andreae, S. G. Warren, Oceanic  
650 phytoplankton, atmospheric sulphur, cloud albedo and climate, *Nature*  
651 326 (6114) (1987) 655–661.
- 652 [17] K. D. Six, S. Kloster, T. Ilyina, S. D. Archer, K. Zhang, E. Maier-  
653 Reimer, Global warming amplified by reduced sulphur fluxes as a result  
654 of ocean acidification, *Nature Climate Change* 3 (11) (2013) 975–978.
- 655 [18] J. Schwinger, J. Tjiputra, N. Goris, K. D. Six, A. Kirkevåg, Ø. Seland,  
656 C. Heinze, T. Ilyina, Amplification of global warming through ph de-  
657 pendence of dms production simulated with a fully coupled earth system  
658 model, *Biogeosciences* 14 (15) (2017) 3633.
- 659 [19] T. W. Wilson, L. A. Ladino, P. A. Alpert, M. N. Breckels, I. M. Brooks,  
660 J. Browse, S. M. Burrows, K. S. Carslaw, J. A. Huffman, C. Judd, et al.,  
661 A marine biogenic source of atmospheric ice-nucleating particles, *Nature*  
662 525 (7568) (2015) 234–238.
- 663 [20] J. Lovelock, *Gaia: A new look at life on earth*, Oxford Paperbacks, 1979.
- 664 [21] J. Lovelock, *The ages of Gaia: A biography of our living earth*, Oxford  
665 University Press, USA, 2000.
- 666 [22] A. Borges, L.-S. Schiettecatte, G. Abril, B. Delille, F. Gazeau, Carbon  
667 dioxide in european coastal waters, *Estuarine, Coastal and Shelf Science*  
668 70 (3) (2006) 375–387.
- 669 [23] R. A. Jahnke, Global synthesis, in: *Carbon and nutrient fluxes in con-  
670 tinental margins*, Springer, 2010, pp. 597–615.
- 671 [24] O. Legge, M. Johnson, N. Hicks, T. Jickells, M. Diesing, J. Aldridge,  
672 J. Andrews, Y. Artioli, D. C. Bakker, M. T. Burrows, et al., Carbon on  
673 the northwest european shelf: Contemporary budget and future influ-  
674 ences, *Frontiers in Marine Science* 7 (2020) 143.

- 675 [25] G. Madec, et al., Nemo ocean engine (2015).
- 676 [26] J. Bruggeman, K. Bolding, A general framework for aquatic biogeochem-  
677 ical models, *Environmental modelling & software* 61 (2014) 249–265.
- 678 [27] J. Bruggeman, K. Bolding, Framework for aquatic biogeochemical mod-  
679 els (2020). doi:<http://doi.org/10.5281/zenodo.3817997>.
- 680 [28] J. Baretta, W. Ebenhöh, P. Ruardij, The european regional seas ecosys-  
681 tem model, a complex marine ecosystem model, *Netherlands Journal of*  
682 *Sea Research* 33 (3-4) (1995) 233–246.
- 683 [29] M. Butenschön, J. Clark, J. N. Aldridge, J. I. Allen, Y. Artioli, J. Black-  
684 ford, J. Bruggeman, P. Cazenave, S. Ciavatta, S. Kay, et al., Ersem  
685 15.06: a generic model for marine biogeochemistry and the ecosystem  
686 dynamics of the lower trophic levels, *Geoscientific Model Development*  
687 9 (4) (2016) 1293–1339.
- 688 [30] P. M. L. Marine Systems Modelling Group, European regional seas  
689 ecosystem model (2020). doi:<http://doi.org/10.5281/zenodo.3817997>.
- 690 [31] J. Skákala, J. Bruggeman, R. J. Brewin, D. A. Ford, S. Ciavatta, Im-  
691 proved representation of underwater light field and its impact on ecosys-  
692 tem dynamics: a study in the north sea, *Journal of Geophysical Re-*  
693 *search: Oceans* (2020) e2020JC016122.
- 694 [32] W. W. Gregg, N. W. Casey, Skill assessment of a spectral ocean–  
695 atmosphere radiative model, *Journal of Marine Systems* 76 (1-2) (2009)  
696 49–63.
- 697 [33] W. W. Gregg, C. S. Rousseaux, Directional and spectral irradiance in  
698 ocean models: effects on simulated global phytoplankton, nutrients, and  
699 primary production, *Frontiers in Marine Science* 3 (2016) 240.
- 700 [34] W. W. Gregg, C. S. Rousseaux, Simulating pace global ocean radiances,  
701 *Frontiers in Marine Science* 4 (2017) 60.
- 702 [35] J. Bruggeman, J. Skákala, J. Lawrence, D. Ford, R. Brewin, S. Ciavatta,  
703 Fabm-spectral (2021). doi:<http://doi.org/10.5281/zenodo.4594277>.

- 704 [36] J. Skákala, D. A. Ford, J. Bruggeman, T. Hull, J. Kaiser, R. R. King,  
705 B. R. Loveday, M. R. Palmer, T. J. Smyth, C. A. J. Williams, S. Cia-  
706 vatta, Towards a multi-platform assimilative system for ocean biogeo-  
707 chemistry, Earth and Space Science Open Archive ESSOAr, submitted  
708 to JGR-Oceans (2021).
- 709 [37] M. J. Lutz, K. Caldeira, R. B. Dunbar, M. J. Behrenfeld, Seasonal  
710 rhythms of net primary production and particulate organic carbon flux  
711 to depth describe the efficiency of biological pump in the global ocean,  
712 Journal of Geophysical Research: Oceans 112 (C10) (2007).
- 713 [38] S. A. Henson, J. P. Dunne, J. L. Sarmiento, Decadal variability in  
714 north atlantic phytoplankton blooms, Journal of Geophysical Research:  
715 Oceans 114 (C4) (2009).
- 716 [39] M. J. Behrenfeld, E. S. Boss, Student’s tutorial on bloom hypotheses  
717 in the context of phytoplankton annual cycles, Global change biology  
718 24 (1) (2018) 55–77.
- 719 [40] J. Huisman, P. van Oostveen, F. J. Weissing, Critical depth and criti-  
720 cal turbulence: two different mechanisms for the development of phyto-  
721 plankton blooms, Limnology and oceanography 44 (7) (1999) 1781–1787.
- 722 [41] J. J. Waniek, The role of physical forcing in initiation of spring blooms  
723 in the northeast atlantic, Journal of Marine Systems 39 (1-2) (2003)  
724 57–82.
- 725 [42] A. Ferreira, H. Hátún, F. Counillon, M. Payne, A. Visser, Synoptic-scale  
726 analysis of mechanisms driving surface chlorophyll dynamics in the north  
727 atlantic, Biogeosciences 12 (11) (2015) 3641–3653.
- 728 [43] J. R. Taylor, R. Ferrari, Shutdown of turbulent convection as a new  
729 criterion for the onset of spring phytoplankton blooms, Limnology and  
730 Oceanography 56 (6) (2011) 2293–2307.
- 731 [44] T. J. Smyth, I. Allen, A. Atkinson, J. T. Bruun, R. A. Harmer, R. D.  
732 Pingree, C. E. Widdicombe, P. J. Somerfield, Ocean net heat flux influ-  
733 ences seasonal to interannual patterns of plankton abundance, PloS one  
734 9 (6) (2014).

- 735 [45] D. A. Ford, J. van der Molen, K. Hyder, J. Bacon, R. Barciela,  
736 V. Creach, R. McEwan, P. Ruardij, R. Forster, Observing and modelling  
737 phytoplankton community structure in the north sea, *Biogeosciences*  
738 14 (6) (2017) 1419–1444.
- 739 [46] J. Skákala, D. Ford, R. J. Brewin, R. McEwan, S. Kay, B. Taylor,  
740 L. de Mora, S. Ciavatta, The assimilation of phytoplankton functional  
741 types for operational forecasting in the northwest european shelf, *Journal of Geophysical Research: Oceans* 123 (8) (2018) 5230–5247.  
742
- 743 [47] E. O’Dea, R. Furner, S. Wakelin, J. Siddorn, J. While, P. Sykes, R. King,  
744 J. Holt, H. Hewitt, The co5 configuration of the 7 km atlantic margin  
745 model: large-scale biases and sensitivity to forcing, physics options and  
746 vertical resolution, *Geoscientific Model Development* 10 (8) (2017) 2947.
- 747 [48] J. Siddorn, R. Furner, An analytical stretching function that combines  
748 the best attributes of geopotential and terrain-following vertical coordi-  
749 nates, *Ocean Modelling* 66 (2013) 1–13.
- 750 [49] D. Storkey, E. Blockley, R. Furner, C. Guiavarc’h, D. Lea, M. Martin,  
751 R. Barciela, A. Hines, P. Hyder, J. Siddorn, Forecasting the ocean state  
752 using nemo: The new foam system, *Journal of operational oceanography*  
753 3 (1) (2010) 3–15.
- 754 [50] H.-J. Lenhart, D. K. Mills, H. Baretta-Bekker, S. M. Van Leeuwen,  
755 J. Van Der Molen, J. W. Baretta, M. Blaas, X. Desmit, W. Kühn,  
756 G. Lacroix, et al., Predicting the consequences of nutrient reduction on  
757 the eutrophication status of the north sea, *Journal of Marine Systems*  
758 81 (1-2) (2010) 148–170.
- 759 [51] J. Blackford, An analysis of benthic biological dynamics in a north sea  
760 ecosystem model, *Journal of Sea Research* 38 (3-4) (1997) 213–230.
- 761 [52] R. Geider, H. MacIntyre, T. Kana, Dynamic model of phytoplankton  
762 growth and acclimation: responses of the balanced growth rate and the  
763 chlorophyll a: carbon ratio to light, nutrient-limitation and temperature,  
764 *Marine Ecology Progress Series* 148 (1997) 187–200.
- 765 [53] J. Baretta-Bekker, J. Baretta, W. Ebenhöf, Microbial dynamics in the  
766 marine ecosystem model ersem ii with decoupled carbon assimilation  
767 and nutrient uptake, *Journal of Sea Research* 38 (3-4) (1997) 195–211.

- 768 [54] Y. Artioli, J. C. Blackford, M. Butenschön, J. T. Holt, S. L. Wakelin,  
769 H. Thomas, A. V. Borges, J. I. Allen, The carbonate system in the north  
770 sea: Sensitivity and model validation, *Journal of Marine Systems* 102  
771 (2012) 1–13.
- 772 [55] H. E. Garcia, R. A. Locarnini, T. P. Boyer, J. I. Antonov, O. K. Bara-  
773 nova, M. M. Zweng, J. R. Reagan, D. R. Johnson, A. V. Mishonov,  
774 S. Levitus, *World ocean atlas 2013. volume 4, dissolved inorganic nutri-  
775 ents (phosphate, nitrate, silicate)* (2013).
- 776 [56] R. M. Key, A. Olsen, S. van Heuven, S. K. Lauvset, A. Velo, X. Lin,  
777 C. Schirnick, A. Kozyr, T. Tanhua, M. Hoppema, et al., *Global ocean  
778 data analysis project, version 2 (glodapv2)* (2015).
- 779 [57] S. K. Lauvset, R. M. Key, A. Olsen, S. van Heuven, A. Velo, X. Lin,  
780 C. Schirnick, A. Kozyr, T. Tanhua, M. Hoppema, et al., *A new global  
781 interior ocean mapped climatology: The 1 × 1 glodap version 2*, *Earth  
782 System Science Data* 8 (2016) 325–340.
- 783 [58] Z.-P. Lee, K.-P. Du, R. Arnone, *A model for the diffuse attenuation  
784 coefficient of downwelling irradiance*, *Journal of Geophysical Research:  
785 Oceans* 110 (C2) (2005).
- 786 [59] T. J. Smyth, Y. Artioli, *Global inherent optical properties from SeaW-  
787 iFS data* (2010). doi:10.1594/PANGAEA.741913.  
788 URL <https://doi.org/10.1594/PANGAEA.741913>
- 789 [60] S. A. Good, M. J. Martin, N. A. Rayner, *En4: Quality controlled  
790 ocean temperature and salinity profiles and monthly objective analyses  
791 with uncertainty estimates*, *Journal of Geophysical Research: Oceans*  
792 118 (12) (2013) 6704–6716.
- 793 [61] J. While, M. J. Martin, *Variational bias correction of satellite sea-surface  
794 temperature data incorporating observations of the bias*, *Quarterly Jour-  
795 nal of the Royal Meteorological Society* 145 (723) (2019) 2733–2754.
- 796 [62] S. Sathyendranath, R. J. Brewin, C. Brockmann, V. Brotas, B. Calton,  
797 A. Chuprin, P. Cipollini, A. B. Couto, J. Dingle, R. Doerffer, et al., *An  
798 ocean-colour time series for use in climate studies: The experience of the  
799 ocean-colour climate change initiative (oc-cci)*, *Sensors* 19 (19) (2019)  
800 4285.

- 801 [63] J. W. Campbell, The lognormal distribution as a model for bio-optical  
802 variability in the sea, *Journal of Geophysical Research: Oceans* 100 (C7)  
803 (1995) 13237–13254.
- 804 [64] A. D. Beaton, C. L. Cardwell, R. S. Thomas, V. J. Sieben, F.-E. Legiret,  
805 E. M. Waugh, P. J. Statham, M. C. Mowlem, H. Morgan, Lab-on-chip  
806 measurement of nitrate and nitrite for in situ analysis of natural waters,  
807 *Environmental science & technology* 46 (17) (2012) 9548–9556.
- 808 [65] A. G. Vincent, R. W. Pascal, A. D. Beaton, J. Walk, J. E. Hopkins,  
809 E. M. S. Woodward, M. Mowlem, M. C. Lohan, Nitrate drawdown dur-  
810 ing a shelf sea spring bloom revealed using a novel microfluidic in situ  
811 chemical sensor deployed within an autonomous underwater glider, *Ma-  
812 rine Chemistry* 205 (2018) 29–36.
- 813 [66] A. Birchill, G. Clinton-Bailey, R. Hanz, E. Mawji, T. Cariou, C. White,  
814 S. Ussher, P. Worsfold, E. P. Achterberg, M. Mowlem, Realistic measure-  
815 ment uncertainties for marine macronutrient measurements conducted  
816 using gas segmented flow and lab-on-chip techniques, *Talanta* 200 (2019)  
817 228–235.
- 818 [67] I. Hinrichs, V. Gouretski, J. Päch, K. Emeis, D. Stammer, North sea  
819 biogeochemical climatology (2017).
- 820 [68] K. Mogensen, M. Balmaseda, A. Weaver, M. Martin, A. Vidard,  
821 Nemovar: A variational data assimilation system for the nemo ocean  
822 model, *ECMWF newsletter* 120 (2009) 17–22.
- 823 [69] K. Mogensen, M. A. Balmaseda, A. Weaver, et al., The nemovar ocean  
824 data assimilation system as implemented in the ecmwf ocean analysis  
825 for system 4 (2012).
- 826 [70] J. Waters, D. J. Lea, M. J. Martin, I. Mirouze, A. Weaver, J. While,  
827 Implementing a variational data assimilation system in an operational  
828 1/4 degree global ocean model, *Quarterly Journal of the Royal Meteo-  
829 rological Society* 141 (687) (2015) 333–349.
- 830 [71] S. Kay, R. McEwan, D. Ford, North west european shelf production  
831 centre northwestshelf\_analysis\_forecast\_bio\_004\_011, quality information  
832 document, Copernicus Marine Environment Monitoring Service (2019).

- 833 [72] R. R. King, J. While, M. J. Martin, D. J. Lea, B. Lemieux-Dudon, J. Wa-  
834 ters, E. O’Dea, Improving the initialisation of the met office operational  
835 shelf-seas model, *Ocean Modelling* 130 (2018) 1–14.
- 836 [73] D. Ford, Assimilating synthetic biogeochemical-argo and ocean colour  
837 observations into a global ocean model to inform observing system de-  
838 sign, *Biogeosciences* 18 (2) (2021) 509–534.
- 839 [74] S. Bloom, L. Takacs, A. Da Silva, D. Ledvina, Data assimilation using  
840 incremental analysis updates, *Monthly Weather Review* 124 (6) (1996)  
841 1256–1271.
- 842 [75] H. Sverdrup, On conditions for the vernal blooming of phytoplankton,  
843 *J. Cons. Int. Explor. Mer* 18 (3) (1953) 287–295.
- 844 [76] M. Goodliff, T. Bruening, F. Schwichtenberg, X. Li, A. Lindenthal,  
845 I. Lorkowski, L. Nerger, Temperature assimilation into a coastal ocean-  
846 biogeochemical model: assessment of weakly and strongly coupled data  
847 assimilation, *Ocean Dynamics* 69 (10) (2019) 1217–1237.